Rijksuniversiteit Groningen

Effect of Heat Treatment and Composition on Electrochemical Behaviour of AISI 420 Martensitic Stainless Steels

by

Sven van der Meer

A thesis submitted in partial fulfillment for the degree of
Master of Science, Applied Physics

at the
Faculty of Mathematics and Natural Sciences

October 2016

rijksuniversiteit groningen

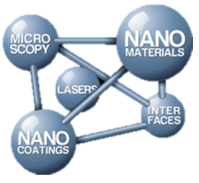

"Information is the oxygen of the modern age. . . . It seeps through the walls topped with barbed wire. It wafts across the electrified, booby-trapped borders. Breezes of electronic beams blow through the Iron Curtain as if it was lace."

Ronald Reagan
June 13, 1989

Abstract

Effect of Heat Treatment and Composition on Electrochemical Behaviour of AISI 420 Martensitic Stainless Steels

by Sven van der Meer

In this research the effect of hardening and tempering temperature, time and environment is studied with use of electrochemical experiments, microscopy and spectroscopy. In this way influence of parameters like, temperature, time, environment and composition on the corrosion resistance could be measured and used to model the AISI 420 martensitic stainless steel. It was found that increasing the tempering temperature decreases the pitting potential due to an increase of carbide formation. By tempering in air surface oxides were grown. For tempering at 250 °C iron oxides are formed on top of the metal surface, which are lowering the current density and affecting the pitting potential. By increasing the tempering time the pitting potential E_{pitt} decreased. Growing chromium oxides by tempering in vacuum at 600 °C the passive behaviour was diminished. The alloying elements nickel and molybdenum stabilize the passive layer but therefore do not effect the pitting potential. Niobium is involved in different mechanisms during the heating stages and increased the OCP but lowered the pitting potential E_{pitt}. Polishing the samples down to 0,25 micron also diminished the passive behaviour during polarization tests, this seems to be caused by a damaged surface after the polishing before testing.

Acknowledgements

First I want to thank ir. Gerrit Zijlstra, PhD candidate at the University of Groningen in the Materials Science Group, for the great cooperation and help during my research project. I was always welcome to brainstorm about new experiments or results and ask questions. He kept me motivated steered me in the right direction when needed. There was always room for jokes and fun, what made working with Gerrit a pleasure. The Fokke and Sukke cartoon shown below was placed on my desk by Gerrit to remind me how to finish my research project. Thank you!

Secondly, I want to thank Prof. Jeff T.M. de Hosson as a supervisor. I was always welcome to ask for suggestions or to comment on results. With this help I was able to explore new paths, helping to find the answers I was looking for. I want to thank him especially for finding an internship I will start hereafter. Without his extensive network and commitment with his students, I would not be able to find this great opportunity.

I also want to thank the complete Materials Science Group, especially David Vainchtein and Václav Ocelík for helping me with the experimental setup and assisting with the use of experimental facilities. I would also like to thank Philips for providing this research project.

Introduction

Stainless steels are defined as iron-based alloys with a significant amount of chromium [1]. Due to the presence of chromium these materials show resistance to corrosion in aqueous environments. For some of these stainless steels other elements are added, like nickel and molybdenum, to improve the corrosion resistance. During the production process of a stainless steel product the steel sometimes undergoes a heating process. This heating process, hardening and tempering, defines the mechanical properties but also influences the corrosion resistance.

In 2014 a stunning 41,7 million metric tonnes of stainless steel was produced. Almost 40% from that is used in metal products [2]. Therefore optimizing the production process and composition of these stainless steel is a subject of high interest. If the underlying mechanisms that define the material properties of these stainless steels are better understood the composition and processing can be precisely tuned and optimized. This will lead to more reliable, sustainable and cheaper products.

This research focuses on the AISI 420 type martensitic stainless steel. This material contains a relative low carbon and chromium concentration, 0,32% and 13,7% respectively. Du to its balance between workability and corrosion resistance, Philips is using this stainless steel for their shavers. Specifically the caps that hold the shaving blades. For production of these caps the AISI 420 steel is processed in 5 stages; forming, hardening, quenching, tempering and finishing. After the heating stages the caps are stored in a controlled environment to avoid corrosion. For this research we focus on the hardening and tempering stage to study the influence of this stage on the final properties of the material with special interest in the corrosion resistance.

By varying the different parameters of these stages, like temperature, time and environment we can see the consequences and unveil the underlying mechanism. Using different techniques like, (electron) microscopy, XPS, EDS and electrochemical testing the material characteristics can be measured and information combined to model the material behaviour. Eventually this information can be used to tune the production process for the caps to improve the quality and or lower the costs.

Contents

Abstract ii

Acknowledgements/Dankwoord iii

Introduction iv

List of Figures vii

1 Corrosion Basics of Metals 1
- 1.1 Reduction and Oxidation . . . 1
- 1.2 Corrosion Electrochemistry . . . 2
  - 1.2.1 Corrosion Potential or Open-circuit Potential . . . 3
  - 1.2.2 Polarization and overpotential . . . 4
  - 1.2.3 Evans Diagram . . . 6
- 1.3 Potentiodynamic Polarization Tests . . . 8
- 1.4 Passivation of Martensitic Stainless Steels . . . 10
- 1.5 Heat Treatment of Martensitic Stainless Steels . . . 11

2 Martensitic Stainless Steels and Passivation 13
- 2.1 Model of Bulk Martensitic Stainless Steel . . . 13
  - 2.1.1 Effects of Austenitizing Temperature on Passive Behaviour . . . 16
  - 2.1.2 Effects of Tempering Temperature . . . 16
- 2.2 Surface Oxides and the Influence of Heat Treatment . . . 17

3 Experimental Setup 19
- 3.1 Avesta Cell for Electrochemical Experiments . . . 19
- 3.2 Sample Preparation . . . 20
- 3.3 Polarization Curves . . . 20
- 3.4 Open-circuit Potential . . . 21

4 Results 23
- 4.1 Carbides and Polarization Testing . . . 23
- 4.2 Surface Oxides and Polarization Testing . . . 24
  - 4.2.1 Iron Oxides . . . 25
  - 4.2.2 Chromium Oxides . . . 28

4.3 Polarization Testing of Different AISI 420 Types 29
4.4 Polarization Testing of Mirror Polished Samples 32

5 Discussion and Conclusion **35**
5.1 Discussion 35
5.2 Conclusions 37
5.3 Future Research 39

Bibliography **41**

List of Figures

1.1 Luggin capillary . . . 4
1.2 Evans Diagram . . . 7
1.3 Evans Diagram Concentration Controlled . . . 8
1.4 Electrochemical Cell . . . 9
1.5 Evans Diagram with Passive Region . . . 9
1.6 Example of Evans diagram with a shift in the OCP due to a decrease in anodic reactivity. (Modified from [3]). . . . 10
1.7 OCP measured in time in 3,5% NaCL aquous solution for samples with different heat treatments. The first number in the legenda gives the austenitizing temperature and the second gives the tempering temperature. [4] . . . 11

2.1 Left: Decreasing number of carbide for increasing hardening/austinitizing temperature for martensitic stainless steel with 0.65% carbon. Right: Phase diagram for Fe-C-Cr martensitic stainless steels. Adapted from [1] . 14
2.2 (a) SEM micrograph with measured line scan from matrix to carbide, (b) iron and chromium percentage in various distance of carbides. [5] . . . 15
2.3 Schematic figure of the corrosion process in cloride rich environments around chromium enriched carbides in martensitic stainless steels. Adapted from [6]. . . . 15
2.4 Effects of Austenitizing . . . 16
2.5 Effects of Tempering . . . 17
2.6 Left: depth profile of SS 304 sample tempered at 200 °C for 2h. Right: depth profile of SS 304 sample tempered at 900 degrees for 2h. [7]. . . . 18

3.1 Schematic figure of Avesta Cell bottom with distilled water inlet to avoid crevice corrosion. . . . 20
3.2 Schematic figure of Avesta Cell with it's electrodes; working electrode or sample, silver/silver chloride reference electrode and platinum counter electrode. . . . 21
3.3 OCP measurement in time after a pretreatment of -0.5V vs Ag/AgCl of a polished AISI 420 sample in 3.5% NaCl solution. . . . 22

4.1 Potentiodynamic polarization curves of AISI 420 samples with different tempering temperatures; as received, 250 °C, 400 °C and 600 °C for 2 hours in 3.5% NaCl aqeous solution at room temperature. . . . 24

4.2 Left: Optical and SEM images of surface of AISI 420 sample after hardening at 1050 °C and before tempering. Right: Optical and SEM images of surface of AISI 420 sample after hardening at 1050 °C and tempering at 300 °C for 2-4 hours. The optical images are from a samples tempered 300 °C for 4 hours. The SEM images are from a samples tempered at 300-400 °C for 50 minutes. 25
4.3 Sample with in the middle a circle of the removed oxide layers by applying -1V potential for 30 minutes. The blank steel next to the gold coloured surface is clearly visible. With EDS the chemical composition is compared. 26
4.4 Potentiodynamic polarization curves of AISI 420 samples hardened at 1050 °C for 45 minutes and tempered at 250 °C for 20 minutes (250-20) and 120 minutes (250-120). Samples were compared polished and unpolished grid 1200 and measured in 3.5% NaCl aqeous solution at room temperature. 27
4.5 Schematic figure of iron oxide grown on top of the passive layer. Due to to this relative thick iron oxide, the depletion zone at the bottom of the well becomes more sensitive for pitting corrosion. The well is seperating the anode and the cathode enhancing pitting corrosion. Adapted from [3]. 28
4.6 Potentiodynamic polarization curves of AISI 420 samples with different surfaces. Both are hardened for 45 minutes at 1050 °C and tempered at 600 °C for 120 minutes in vacuum. The polarization curve of the grinded sample is given in blue and the not grinded sample with the chromium oxide layer is given in red. Measurements were done in 3.5% NaCl aqeous solution at room temperature. 29
4.7 XPS spectrum from AISI 420 sample tempered at 600 °C in vacuum for 80 minutes. The energy ranges for oxygen, iron and chromium are shown respectively. From the peaks it was confirmed that chromium oxides were present at the surface where no iron oxides were measured. 30
4.8 Potentiodynamic polarization curves of AISI 420 samples of different types hardened at 1050 °C for 45 minutes. Samples were grinded up to grid 1200 and measured in 3.5% NaCl aqeous solution at room temperature. 31
4.9 Potentiodynamic polarization curves of AISI 420 samples hardened at 1050 °C for 45 minutes (label: 1050) or used as received (label: AR). Mirror Polished was done beforetempering at 250 °C for 20 minutes (label: 250). Measured in 3.5% NaCl aqeous solution at room temperature. . . . 33
4.10 Mirror polished (1/4 micron) surface of AISI 420 sample before and after a polarization test was done. 34

Chapter 1

Corrosion Basics of Metals

In this chapter the basics about corrosion and stainless steels will be discussed. Furthermore some used techniques will be explained to measure the electrochemical characteristics of stainless steels. Lastly the heat treatment of martensitic stainless steels and its influence on the material properties will be elaborated.

1.1 Reduction and Oxidation

Corrosion is based on the oxidation and reduction process of atoms. At one side there is the process of atoms loosing electrons what is called *oxidation* On the other side we have electrons that are added to the atom. This gaining in negative charge is called *reduction*. Probably the most well known form of corrosion is rust. Rusting occurs when for example iron is exposed to oxygen and water, bringing it back to the mineral form in which it is found in nature; *hydrous ferrous oxide* ($Fe_2O_3 \cdot H_2O$), *hydrated magnetite* ($Fe_3O_4 \cdot H_2O$) or *magnetite* (Fe_3O_4) [3].

For corrosion of metals in aqueous environments the concentration of H^+ and OH^- ions is important. These concentrations are expressed in the acidity or alkalinity (pH) level. This pH level is given by:

$$pH = -log_{10}(a_{H^+}) \tag{1.1}$$

The pH level influences the corrosion process of the metal. For high concentrations of H^+ (low pH levels), atoms like iron (Fe), zinc (Zn) and aluminium (Al) react with the hydrogen atoms present in the solution creating hydrogen gas. For high concentration

of OH^-, ions can react with these metals to form oxides in solid form. Below both reactions are given for iron.

$$Fe(s) + 2H^+(aq) \rightarrow Fe^{2+}(aq) + H_2^0(g) \tag{1.2}$$

$$4Fe(s) + 6H_2O(l) + 3O_2(g) \rightarrow 4Fe(OH)_3(s) \tag{1.3}$$

1.2 Corrosion Electrochemistry

In electrochemical reactions a transfer of electrons is involved by reduction and oxidation. This transfer of electrons can be used as a power source (batteries). An example of this is the Daniel cell where two different metals are placed separated from each other in a solution of their salts and connected with a wire [3]. When one of metals more readily loses electrons a useful current can flow that can be used as a power source. To maintain the charge flow a salt bridge is used. This bridge contains ions to complete the circuit of charge flow. An example of two metals that can be used in a Daniel cell are zinc and copper. In this case the zinc will function as the anode and lose electrons. The copper will take up electrons and so function as a cathode. The two half reactions of this electrochemical process are given by:

$$Zn(s) \rightarrow Zn^{2+} + 2e^- \tag{1.4}$$

$$Cu^{2+} + 2e^- \rightarrow Cu(s) \tag{1.5}$$

From the amount of electrons that are transferred, the current, one can calculate how many atoms of the metal on the anode are dissolved. In this way the corrosion speed can be calculated from the current in the electrochemical cell with use of *Faraday's law*. According to Faraday's law, 1 mole of electrons is required for the reaction with 1 mole of silver ions. 1 mole of electrons is defined as 1 faraday (F) and equals 96.485 C/mole.

$$Ag^+ + e^- \rightleftharpoons Ag(s) \tag{1.6}$$

The total charge can be calculated by integrating the current over time, with I for the current. From this one can calculate change in the amount of metal Δ N in moles,

$$Q = \int_0^t I \cdot dt = F \cdot \Delta N \cdot n \tag{1.7}$$

where n is is the number of electrons per molecule of the species being reacted. This gives the corrosion speed. In table 1.1 the conversion units for the corrosion speed is given for steel where the conversion factors are adopted to iron (Fe), using $n = 2$, Atomic Mass $M = 55.85g/mol$ and density $d = 7.88gcm^{-3}$

	$mA\ cm^{-2}$	$mm\ y^{-1}$	$g\ m^{-2}\ day^{-1}$
$mA\ cm^{-2}$	1	11.6	249
$mm\ y^{-1}$	0.0863	1	21.6
$g\ m^{-2}\ day^{-1}$	0.00401	0.0463	1

TABLE 1.1: Conversion between Current, mass loss and penetration rates for steel [3]

1.2.1 Corrosion Potential or Open-circuit Potential

The half reactions (1.4) and (1.5) enable a current flow. When the half reactions are known one can predict the current flow in electrochemical cells by using the *standard electrode potentials* of half reactions at both electrodes. The electrons will always flow from the least positive electrode potential to the most positive electrode potential. The two electrode potentials combined give the cell potential. An example of the copper-zinc electrochemical cell is given. The standard electrode potentials of zinc (Zn) and copper (Cu) are -0.7628 V and 0.3402 V respectively [8]. The total cell potential is given by:

$$E_{cell} = E_{cathode} - E_{anode} \tag{1.8}$$

For measuring potentials across an electrochemical cell a historically important reference cell is the standard hydrogen electrode (SHE). However, these days many other reference electrodes are used for practical uses like the *silver/silver chloride reference electrode* or the *saturated calomel electrode* (SCE). These reference cells are compared with the SHE that by definition has a potential of zero at any temperature.

For corrosion studies the potential of a corroding metal is probably one of the most important variables to measure because the corrosion potential gives the balance between the oxidation and reduction reactions. Usefull information to predict the behaviour of the material in different environments. So measuring the voltage difference between a metal in its environment and a reference electrode and gives the *corrosion potential* or the *open-circuit potential*. Since the potential of the reference electrode is known, the potential of the measured metal can be determined by subtracting the potential of the reference electrode from the measured potential according formula (1.8). The reference cell electrode is brought close to the surface of the measured metal with use of a

Luggin capillary (figure 1.1) [9]. This prevents diffusion of ions between the environment and the solution in the reference electrode what would distort the results. Extensive research is done on the effects of the dimension and position of the Luggin capillary on electrochemical measurements [10]. A rule of thumb is the Luggin capillary shouldn't be placed closer then twice the diameter of the capillary to avoid screening the sample from the current flow. With use of a capillary measurements of the potential can be done close to the surface, giving a more accurate surface measurement.

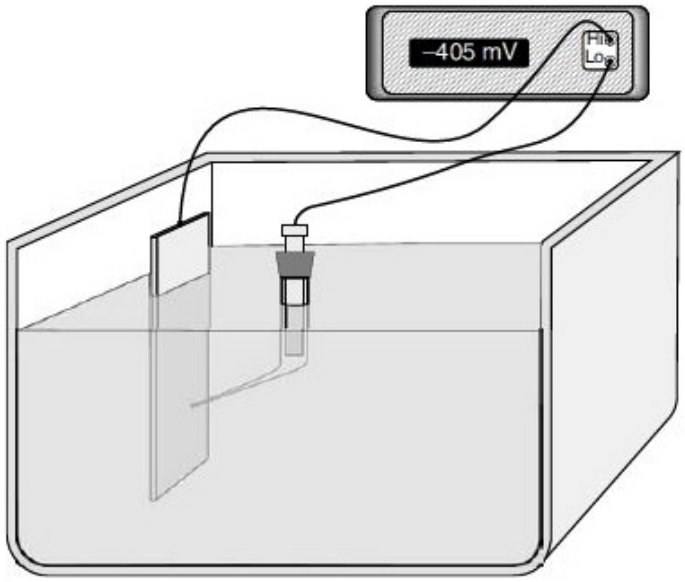

FIGURE 1.1: Meausuring electrode potential with use of reference electrode and Luggin capillary [3]

1.2.2 Polarization and overpotential

The so-called *polarization effects*, control corrosion. This polarization gives rise to the currents in the cathodic and anodic reactions processes. The corrosion potential is a accommodation between the equilibrium potentials of all anodic and cathodic reactions involved. This gives rise to a certain potential E. Nernst [11] defined the difference between resultant potential E and each equilibrium potential of the different half reactions as the *polarization* [11–13]. This polarization is quantified in terms of the *overpotential* η given by:

$$\eta = E - E_{eq} \tag{1.9}$$

When the polarization is anodic this means that anodic reactions are activated for moving the potential to the positive direction. When the cathodic processes are accelerated

for moving the potential in the negative direction, the polarization is called cathodic. An example of cathodic processes is hydrogen formation on iron. When the polarization is cathodic the deteriorating anodic processes are suppressed and the iron is protected, known as cathodic protection. The total function for the polarization is a sum of three distinct types of polarization [3, 14].

$$\eta_{total} = \eta_{act} + \eta_{conc} + iR \tag{1.10}$$

- η_{act} is the *activation overpotential*, depends on the charge transfer and thus on the electrode-electrolyte interaction. The activation overpotential η_act is the main polarization component for small polarization currents or voltages.
- η_{conc} is the *concentration overpotential*, a function describing the mass transport limitations for the electrochemical processes and therefore only significant at larger currents.
- iR is the *ohmic overpotential*. The resistance of the electrolyte causes an ohmic drop. By increasing the ionic conductivity and a small electrolyte thickness is desired to evanesce the contribution of the ohmic polarization.

In most cases the activation polarization is the controlling factor in corrosion processes in strong acids. However, concentration polarization can become dominant in diluted acids for example where the active species are present in low levels. The ohmic drop becomes important for situations where the anodic and cathodic corrosion sites are separated and so the resistance of the electrolyte is important.

Activation Polarization

The *activation polarization* refers to the factors that are inherent to the kinetics in electrochemical reactions [3]. The most important factor is the exchange current density i_0 that defines the rate of oxidation or reduction. This current density is given as the amount of electrical current per cross sectional area of the material. An electrochemical reaction results from a number of successive steps. For example the evolution of hydrogen gas described by:

$$2H^+ + 2e^- \rightarrow H_2(g) \tag{1.11}$$

The rate of the hydrogen formation depends on several factors with the electron transfer from the electrode to the hydrogen as the most important. This rate is defined by the exchange current density. This exchange current density differs for different metal

surfaces. The reaction for what the energy barrier is the lowest wil be predominant. Mercury was often added to power cells since the exchange current density of gaseous hydrogen is 10^{-2} A/m^2 on platinum while its is 10^{-13} A/m^2 on mercury . Therefore the evolution of gaseous hydrogen is much less favorable and makes the battery saver [15]. However because of the toxicity the sale of mercury containing cells is banned [16].

1.2.3 Evans Diagram

Corrosion polarization measurements are represented in a so called Evans Diagram. The polarization curves in this diagram are used to describe the different corrosion processes. According to the mixed potential theory this polarization curve is a sum of the reduction and oxidation reactions. This means that the measured polarization curve comes from all the electrochemical reactions that are acting. So to model the corrosion behavior of the material therefore the activation potential of each corrosion process involved should be known and additional information as concentration dynamics for example that influences the corrosion processes.

For processes that are purely controlled by activation polarization the cathodic and anodic processes can be described with straight lines on the E versus $log(i)$ scale. The gradient of this line is the Tafel coefficient b. Given as:

$$b = \pm 2.303 * \frac{RT}{\beta nF} \tag{1.12}$$

With +2.303 for cathodic reactions and -2.303 for anodic reactions.

- β is the charge transfer barrier or symmetry coefficient, normally close to 0.5
- n is the number of electrons acting in all the reactions
- R is the gas constant (8.314 $[Jmol^{-1}K^{-1}]$)
- T is the temperature in Kelvin
- F is the Faraday constant (96.485 $[C/mol\ of\ electrons]$)

In figure 1.2 the polarization curve of carbon steel is given in a deaerated electrolyte. Clearly the transition from the anodic to the cathodic reaction can be seen as the potential becomes less negative. For a large negative potential many electrons are available at the working electrode (the carbon steel sample) and therefore the formation of hydrogen gas is favorable. This can be seen in the graph because the current density is high at

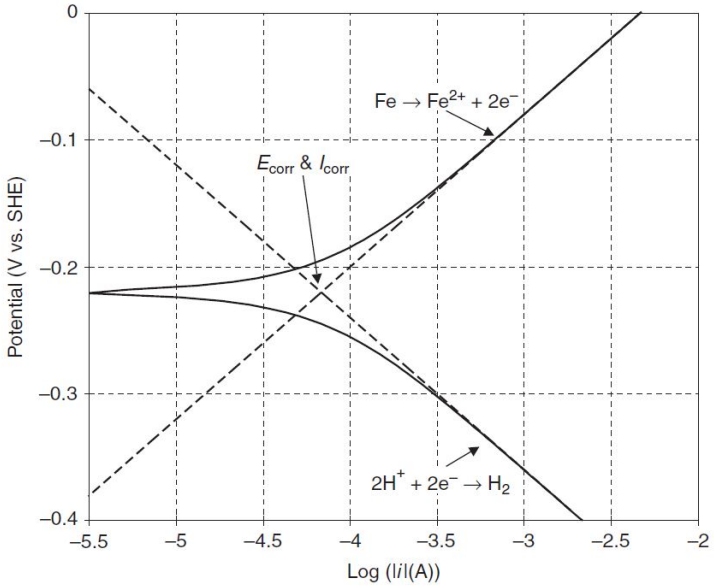

FIGURE 1.2: Polarization curve of carbon steel in deaerated electrolyte showing the anodic and cathodic processes [3].

large negative potentials. When the applied potential becomes less negative this current decreases up to the corrosion potential. This is the point where anodic and the cathodic reaction have an equal activation polarization (the dotted lines cross) and so the current is equal in both directions. The potential at this point is called the corrosion potential and is visible in the graph as a peak that corresponds to a current that goes to zero.

When concentrations of oxygen in the electrolyte influences the electrochemical processes it can be seen in the polarization curve. In the example of carbon steel this can be shown if the process of water formation is included, given by:

$$O_2 + 4H^+ + 4e^- \rightarrow 2H_2O \tag{1.13}$$

When this process is controlled by the oxygen concentration, the current density for this process will not depend on the applied potential and hence will be given by a vertical line in the Evans Diagram. This will change the polarization curve for the potential region where the formation of water is favoured. This can be seen in figure 1.3.

Because the aeration makes the formation of water a favourable process in the transition region for the anodic process of hydrogen formation and the cathodic process of iron oxidation the corrosion potential E_{corr} shifts upwards.

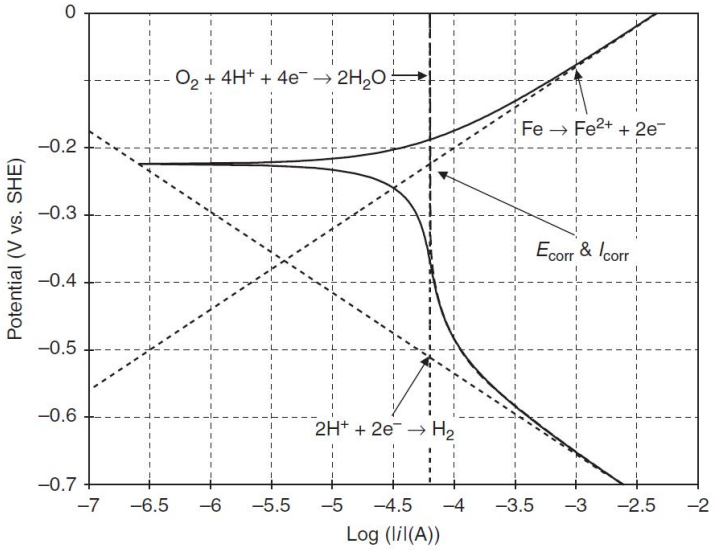

FIGURE 1.3: Polarization curve of carbon steel in aerated electrolyte showing the anodic and cathodic processes that are influenced by the concentration of oxygen. The dotted line represents the Tafel coefficient. [3].

1.3 Potentiodynamic Polarization Tests

There are several ways to study the corrosive behavior of a meterial in its environment by using the previous discussed electrochemical behavior. Most methods are based on applying a current or potential in an electrochemical cell and measure the response of the potential or current respectively. The electrochemical cell consists of three electrodes; the reference electrode, the working electrode or sample and the counterelectrode. The potential or current is applied between the working electrode and the counter electrode and compared to the electrochemical potential of the reference electrode. This setup is schematically shown in figure 1.4.

In the case of potentiodynamic polarization testing the applied potential is increased in steps over a potential range with a fixed step rate $[V/s]$. When this potential is sweeped through the range, starting below the corrosion potential E_{corr} and increased from there, the polarization curve will show a passive region for passivated metals. This is caused by a thin metal oxide layer of a few nanometers that has formed on the metal surface [17, 18]. This oxide layer protects the metal surface from corrosion since these metal oxide layers are bad conductors and hence electron transfer is reduced significant. In this way corrosion processes that degrade the metal are limited. The passivation for stainless steels and the electrochemical effects will be discussed in section 1.4.

When a passive layer has grown on the metal surface that is under investigation, the polarization curve will show a low current density (I_p) in a certain positive potential range respective to the corrosion potential E_{corr}. This is shown in figure 1.5.

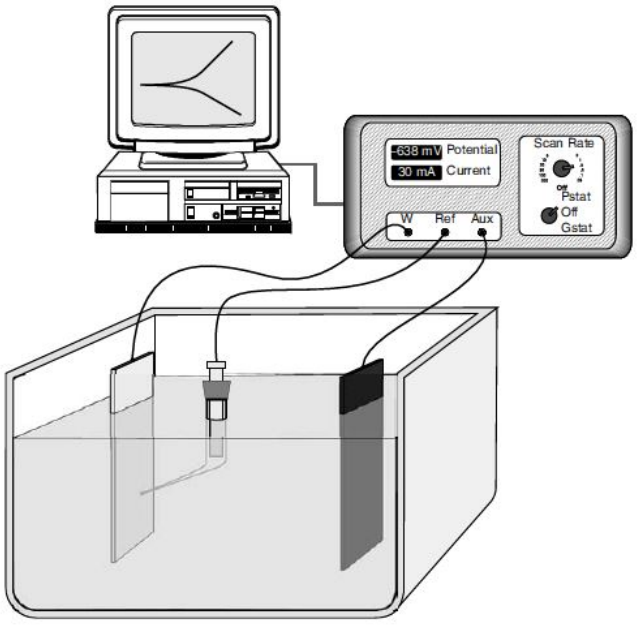

FIGURE 1.4: Schematic representation of an electrochemical cell to do corrosion testing [3].

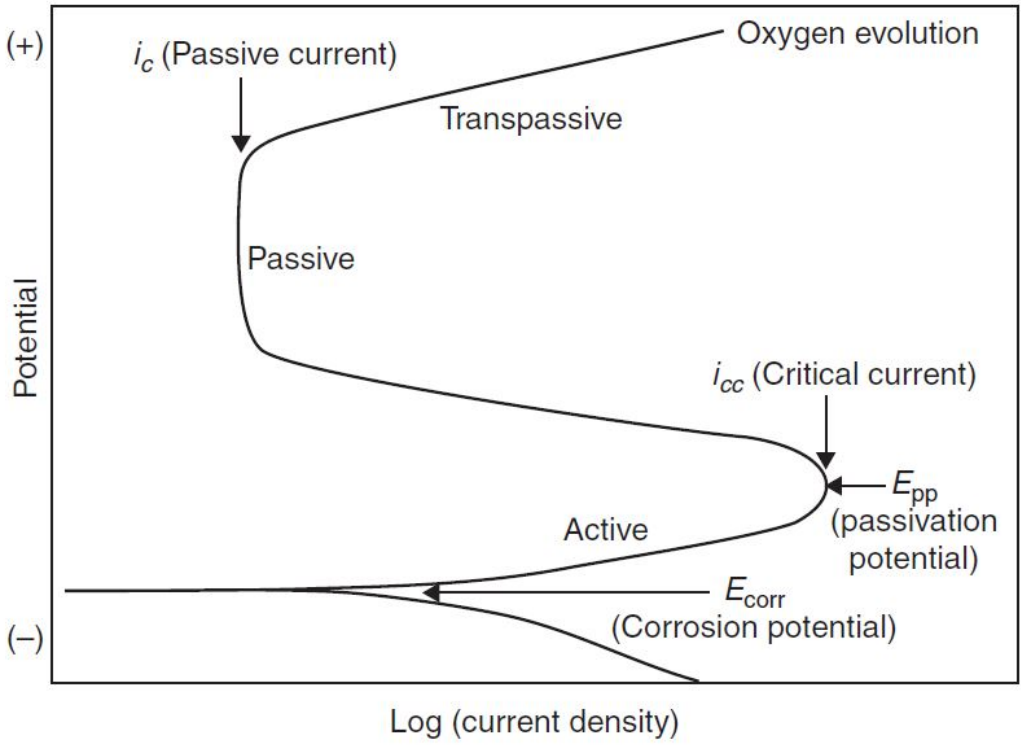

FIGURE 1.5: Example of Evans diagram containing a passive region for higher applied potentials [3].

In this way potentiodynamic polarization measurements can be used to do comparison tests for the passivation of stainless steels. The potential where the passive protection

breaks down and pitting corrosion is initiated is the pitting potentials E_{pitt}. Martensitic stainless steels are an example of the materials that show this passive behaviour and will be discussed below.

1.4 Passivation of Martensitic Stainless Steels

A metal is passive when the steady rate of anodic dissolution for a metal in a given environment is lower for more noble/positive potentials applied [19]. This can be recognized in an Evans diagram shown in figure 1.5. When the potential exceeds the *passivation potential* E_{pp} the current density decreases. As discussed this is a measure for less electron transfer and hence anodic dissolution of the metal.

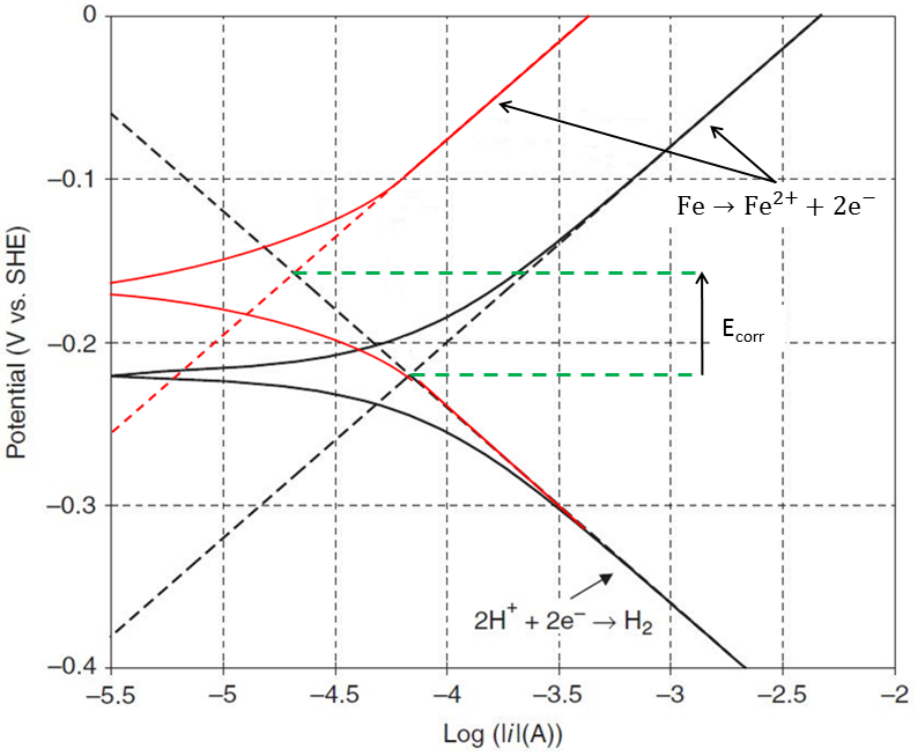

FIGURE 1.6: Example of Evans diagram with a shift in the OCP due to a decrease in anodic reactivity. (Modified from [3]).

Stainless steels show passivity due to an oxide layer that is formed on the surface of the bulk metal. This oxide layer is several nanometers thick and acts as a boundary for electron transfer and decreases anodic reactivity [17, 18]. This means that the passive layer influences the *open-circuit potential* (OCP) or *corrosion potential*. When the anodic reactivity is increased the corrosion potential will shift to more negative potentials and vice versa. This can be explained in the same manner as the influence of the oxygen

concentration. The cathodic reactivity stays the same, independent of the passivity of the stainless steel. However when the passive layer grows the anodic reactivity decreases. This shifts the anodic line to a more negative current density. This shift is shown in figure 1.6.

By monitoring this OCP in time one can study the growth or dissolution of the passive layer of stainless steels [4, 20, 21]. Lu et al. [22] showed that different heat treatments have effect on the passivation process of martensitic stainless steels. In figure 1.7 the results are shown of OCP measurements in time. From this Lu et al. [4] concluded that where the sample with a heat treatment of 1030-500 (austinitizing temperature of 1030 degrees Celsius and tempering of 500 degrees Celcius) first grows a passive layer but then show a breakdown and starts corroding. This breakdown occurs after 300 second where the OCP starts decreasing.

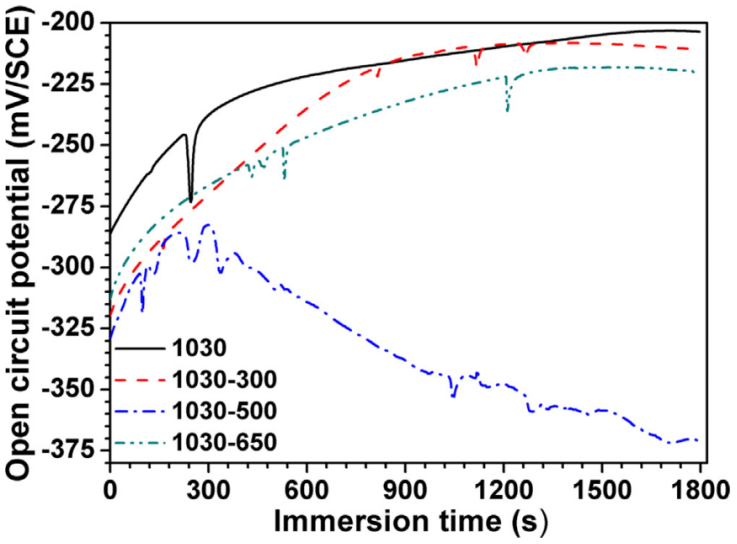

FIGURE 1.7: OCP measured in time in 3,5% NaCL aquous solution for samples with different heat treatments. The first number in the legenda gives the austenitizing temperature and the second gives the tempering temperature. [4]

1.5 Heat Treatment of Martensitic Stainless Steels

Martensitic stainless steels (MSSs) typically undergo two types of heat treatments in the production process before they have the final desired properties; austenitizing (hardening) and tempering.

Semi-finished products undergo *hardening* or *austenitizing* heat treatment. For this heat treatment the steel must be heated to elevated temperatures so that the crystal structure of the iron transform from BCC (body-centered cubic) to FCC (face-centered

cubic). This transformation of iron from ferrite phase to austenite phase allows more carbon dissolute into the matrix [23]. When the austenite is cooled with a high rate, transformation to martensite takes place, this makes the steel very hard. This is why the process is called austenitizing or hardening. The cooled steel has a BCT (body-centered tetragonal) crystal lattice [24].

After austenitizing the steel the next step in the heat treatment is tempering. With tempering the residual stress is removed and toughness increases. Depending on the desired properties the tempering temperature and time can be varied. The tempering temperature should be higher than the working temperature to transform the metastable martensitic phase into more stable tempered phases [4]. The tempering process allows carbide to form and grow and remove retained austenite. By choosing the temperature for tempering carefully the desired properties of the steel can be achieved by balancing strength, toughness and corrosion resistance. Since this last property is of main interest for this report. For further information on this subjec Surpi et al. [1], Isfahany et al. [5], Reed-Hill and Abbaschian [24] are suggested for mechanical properties depending on heat treatment temperatures.

Chapter 2

Martensitic Stainless Steels and Passivation

This research focuses on the AISI 420 type martensitic stainless steel (MSS). Philips is using this stainless steel for their shavers. These MSSs contain typical around 13 wt% Cr. These steels are prepared by heat treatment, containing austenitization and tempering to get the desired mechanical properties. During these processes of heat treatment also the electrochemical properties of the surface are changing, leading to a change in corrosion resistance. Lu et al. did a thorough research on these effects of heat treatment [4, 6, 22, 25]. To understand and improve characteristics of the stainless steel we need a model that describes and explains its behaviour of the surface. The model that will be stated in this chapter is based on two coupled phenomena; the influence of the structure of the bulk material and the oxide layer(s) on this bulk material. Especially effect of heat treatment on this bulk material and possible oxide layers that are grown during this production step are discussed to be able to explain the results found during this research.

2.1 Model of Bulk Martensitic Stainless Steel

Besides iron (Fe), the bulk material of martensitic stainless steels (MSSs) mainly contains carbon (C) and chromium (Cr). These steels contain typically 11.5-18 wt% chromium and 0.1-1 wt% carbon [1]. As described in section 1.5, semi-finished MSSs products undergo two heating treatments: hardening and tempering. These heat treatments influence the final mechanical behaviour but also the corrosion resistance. To understand this a model is given of the bulk material and the influence of heat treatment.

As generally known the diffusion of atoms in solids highly depends on the temperature as found by Arrhenius in 1889 [26]. Following his equation the diffusion coefficient D is given by:

$$D = D_0 e^{-E_A/kT} \tag{2.1}$$

with D_0 for the maximum diffusion coefficient for infinite temperature, E_A for the activation energy, k as the Boltzmann constant and T the temperature.

This means that hardening at higher temperatures enhances uniform distribution of the carbon and chromium in the iron matrix (figure 2.1 left). From the phase diagram of MSSs (figure 2.1 right) with 13% Cr, we see that the steel is completely in austenite phase (γ) with dissoluted carbon and chromium between 950 °C and 1400 °C depending on the carbon concentration. For the AISI 420 stainless steel that is used in this research the carbon concentration is 0.32% this lies roughly between 1100 °C and 1350 °C.

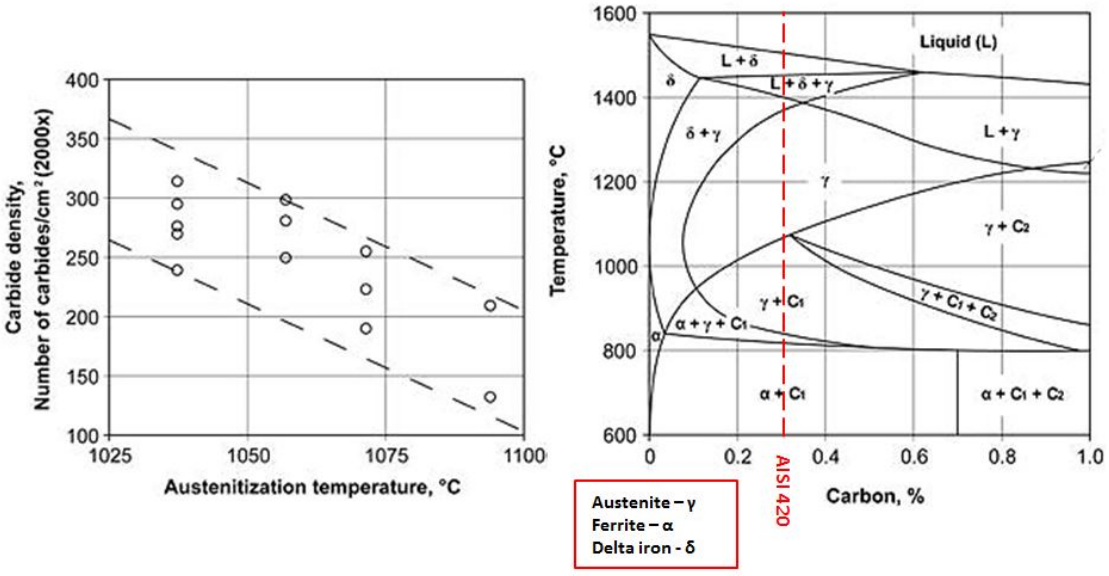

FIGURE 2.1: Left: Decreasing number of carbide for increasing hardening/austinitizing temperature for martensitic stainless steel with 0.65% carbon. Right: Phase diagram for Fe-C-Cr martensitic stainless steels. Adapted from [1]

Carbides in these martensitic stainless steels are chromium enriched, as can be seen in the line scan in figure 2.2 [5]. The formation of these Cr enriched carbides during the annealing or tempering stage in the heat treatment, causes chromium depletion zones around the carbides [6]. Stainless steels are defined as iron-chromium alloys with at least 10.5% chromium [1]. However, studies showed that the passive behaviour of stainless is sometimes already lost with chromium concentrations below 12% [27, 28]. This means that the Cr depletion zone around carbides can retard the formation of the

protective passive film. Therefore the volume at the number of carbides present at the surface of the MSSs are of big influence on the passive behaviour, consequently the heat treatment directly influences the corrosion resistance of the final product. The model of the corrosion process, suggested by Lu et al. is schematically shown in figure 2.3.

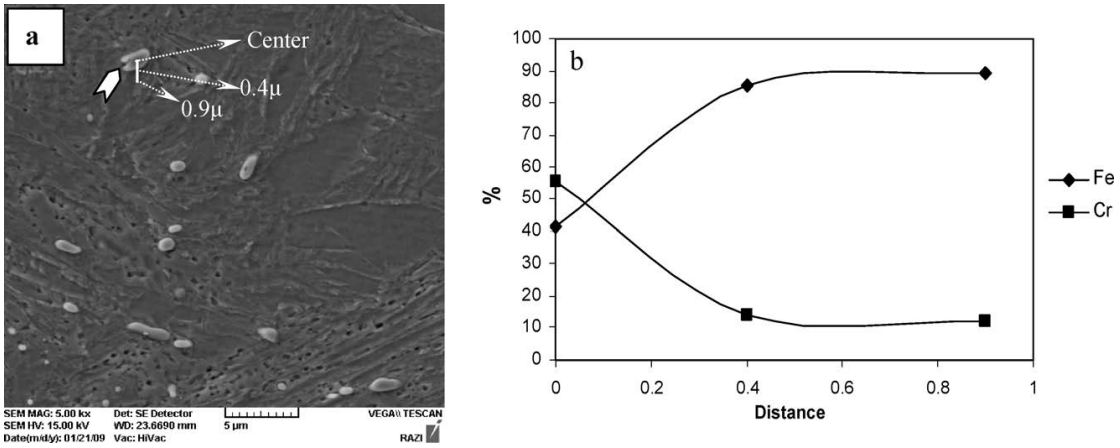

FIGURE 2.2: (a) SEM micrograph with measured line scan from matrix to carbide, (b) iron and chromium percentage in various distance of carbides. [5]

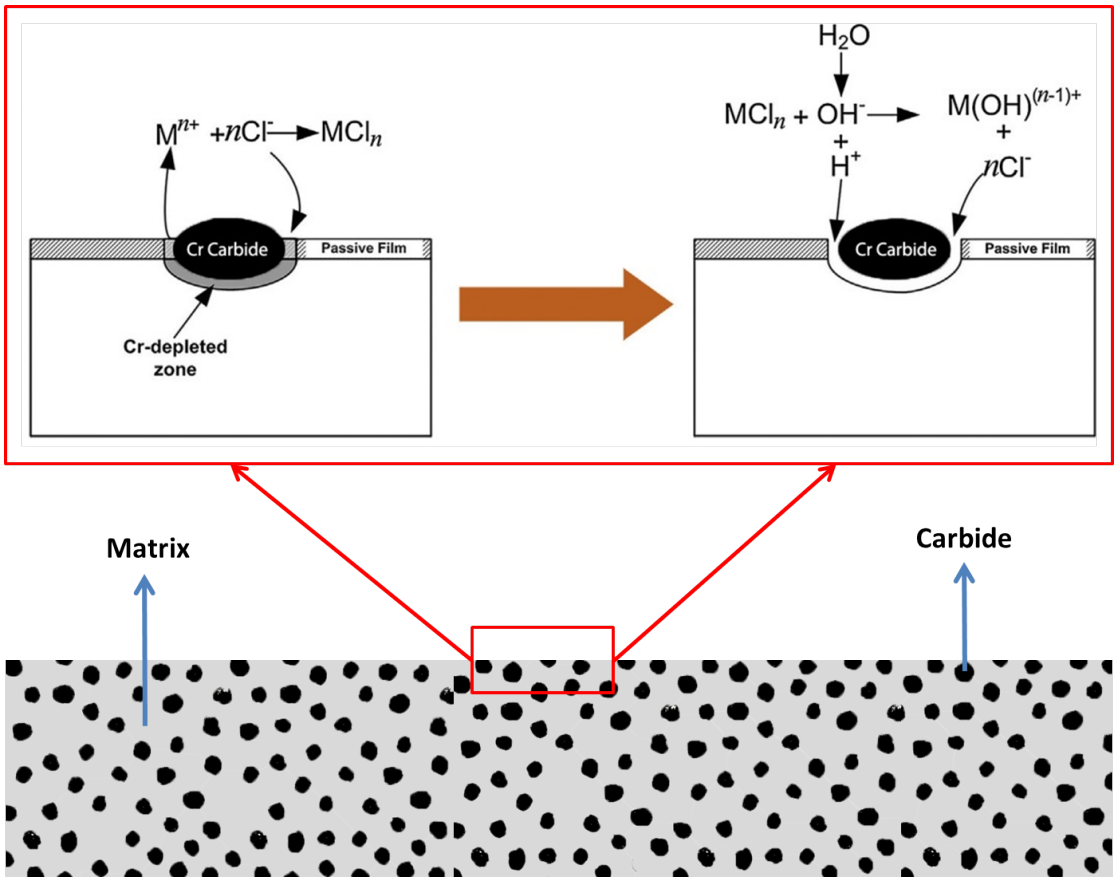

FIGURE 2.3: Schematic figure of the corrosion process in cloride rich environments around chromium enriched carbides in martensitic stainless steels. Adapted from [6].

2.1.1 Effects of Austenitizing Temperature on Passive Behaviour

Withj increasing austenitizing temperatures the carbides dissolve into the matrix, leading to more homogenity in the chromium distribution. Lu et al. [22] measured the polarization behaviour for various austenitizing temperatures. When the passive layer breaks down the current density will suddenly increase indicating pitting corrosion.

Lu et al. [22] studied this passive region and the corresponding pitting potential for martensitic stainless steel (MSS) with a chemical composition (in wt%) of 0.38 C, 0.60 Mn, 0.90 Si, 13.60 Cr, 0.30 V and Fe. From figure 2.4 an increase of the pitting potential E_{pitt} for increasing austenitizing temperatures can be observed. This suggests that the passive layer is stronger when the metal is austenized at higher temperatures. Lu et al. [22] attribute this to dissolution of Cr enriched carbides, improving the chromium homogeneity.

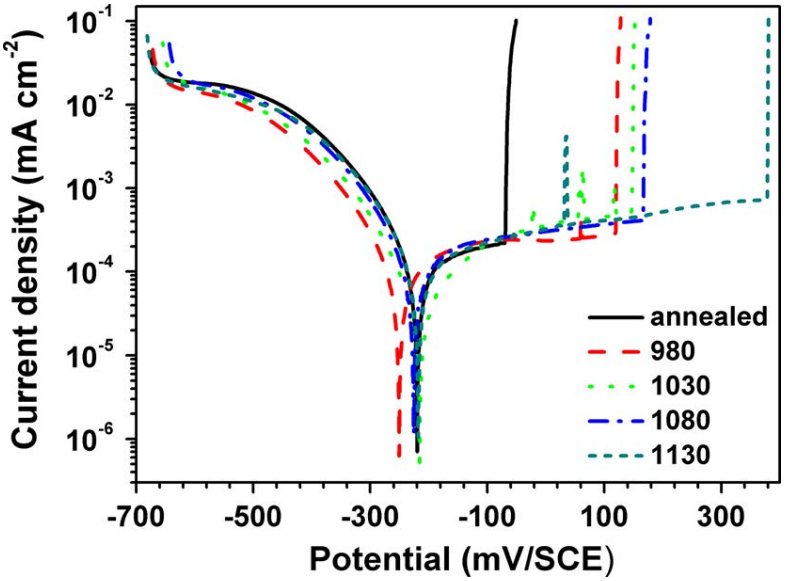

FIGURE 2.4: Potentiodynamic polarization curves for different austenitizing temperatures of experimental stainless steels in 3.5 wt% NaCl at room temperature [22].

2.1.2 Effects of Tempering Temperature

The secondary step in the heat treatment is tempering, typical at a temperature between 300-600 °C for around 1-2 hours. During this process carbides are grown for an optimal strength and toughness at the working temperature, which should be below the tempering temperature. However the formation of carbides will create a chromium depleted zone causing pitting sensitization. This makes the tempering a delicate process to get the desired mechanical and electrochemical properties. Lu et al. [4] measured the polarization curves for different tempering temperatures of MSSs to measure its

passive behavior and the pitting potential. The results are shown in figure 2.5. From this results it was concluded that indeed increasing tempering temperatures up to 500 °C (1030-500) breaks down the passive behavior and therefore decreasing the pitting potential, meaning that the surface becomes more sensitive to pitting corrosion. For even higher tempering at 650 °C (1030-650) the passive behavior is restored partially. Lu et al. suggested that this is correlated to the interspace between, and the sizes of, the carbides formed during tempering:

"For the 1030-500 sample, the interspaces between the nano-sized carbides are smaller than that between the micron-sized carbides in the 1030-650 sample. Therefore, with the same volume fraction, much smaller interspaces between the nano-sized carbides makes the Cr-depleted zone around the carbides more close to each other and in a larger density, consequently hamper the formation of the protective passive films on MSSs." [4]

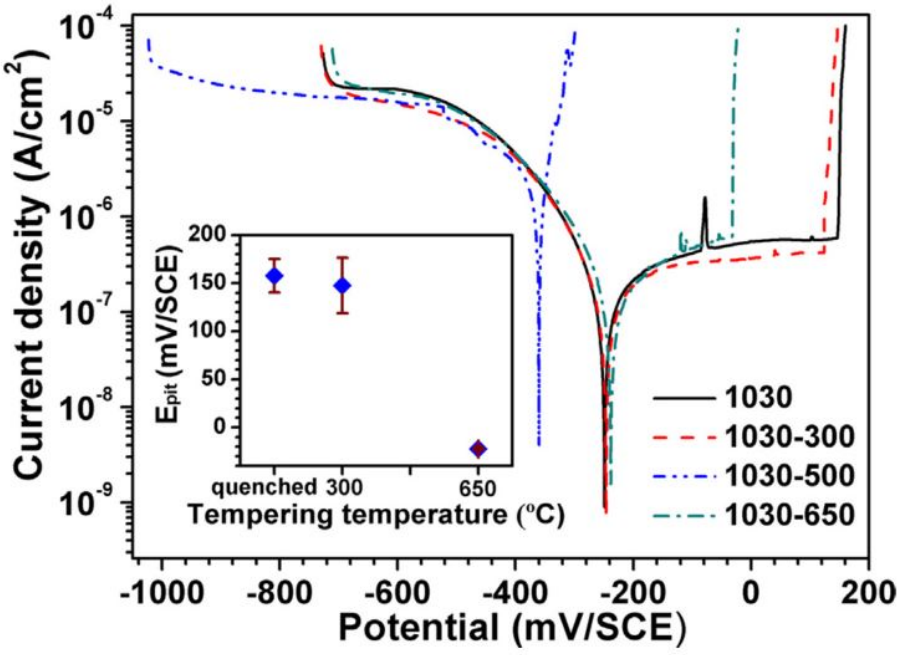

FIGURE 2.5: Potentiodynamic polarization curves of experimental stainless steels in 3.5 wt% NaCl at room temperature for varying tempering temperatures [4].

2.2 Surface Oxides and the Influence of Heat Treatment

Besides the heat treatment has the effects on the martensitic stainless steel itself, it has also effects on the surface composition. Specifically: the heat treatment can cause different types of oxide layer growth on the surface. In this research heat treatment was done in air, the inert gas argon or vacuum between 200 °C and 600 °C. For stainless

steels the surface layers generally consists of Fe and Cr oxides with an outermost film of bound water or oxyhydroxides [18, 29, 30]. When austenite stainless steel is tempered in air, iron oxides will be formed additionally [7, 30]. Betz et al. [7] showed that tempering in air creates iron oxides on top of the chromium enriched passive layer for temperatures between 200-600 °C. From 700 °C chromium oxides start to form and at 900 °C the chromium oxide layer almost fully replaced the iron oxide. The depth profiles of a stainless steel sample at 200 °C and 900 °C for 2 hours is shown in figure 2.6. For the 900 °C tempered sample chromium(oxide) is clearly present, where for the 200 °C iron(oxide) is present.

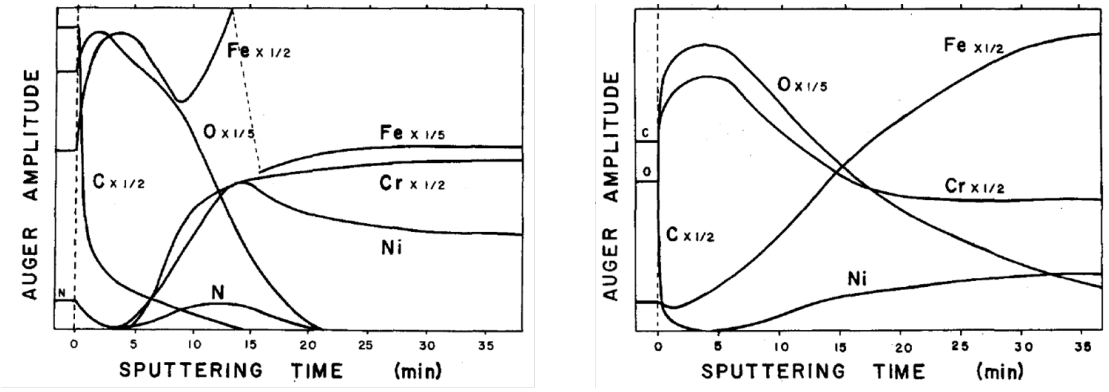

FIGURE 2.6: Left: depth profile of SS 304 sample tempered at 200 °C for 2h. Right: depth profile of SS 304 sample tempered at 900 degrees for 2h. [7].

Chapter 3

Experimental Setup

To understand the surface oxidation of AISI 420 stainless steel and its passive behaviour electrochemical experiments were conducted. In addition optical microscopy and electron microscopy was used to study the surface of the samples. Furthermore X-ray photoelectron spectroscopy (XPS) and Energy-dispersive X-ray spectroscopy (EDS) was used to do chemical characterization of the samples. Samples were made from AISI 420 steel, the composition of this stainless steel is shown in table 3.1.

Chemical composition AISI 420 stainless steel (%)

C	Si	Mn	P	S	Cr
0.32	0.15	0.30	$\leq$0.025	$\leq$0.010	13.7

TABLE 3.1

Electrochemical measurements were conducted with an Avesta electrochemical cell [31, 32]. This three-electrode cell is designed for experiments on pitting corrosion of flat passive metals. Usually crevice corrosion caused problems in experiments on pitting corrosion. Crevice corrosion can be present in the space (crevice) filled with electrolyte between the sample and the mounting material. This type of corrosion causes early breakdown of the passivity and is therefore affects the accuracy of the experiment. Avesta designed a cell that replaces the electrolyte by distilled water in the (micro)crevices between the sample and the mounting material to avoid crevice corrosion.

3.1 Avesta Cell for Electrochemical Experiments

The design of the Avesta Cell is such that in pitting corrosion tests crevice corrosion is avoided. This is done by an continuous flow of distilled water between the sample

surface and the mounting material of the cell. In figure 3.1 the cell bottom is shown in a schematic figure. The distilled water is pumped in the filter paper ring that fills the space between the cell bottom and the sample. The pump ratio is around 5 ml/h, high enough to prevent crevice corrosion but too low for significant dilution since measurements take around 2 hours and the cell contains is filled with 500 milliliters of electrolyte. The rubber O-ring prevents the cell from leaking distilled water to the outside of the cell.

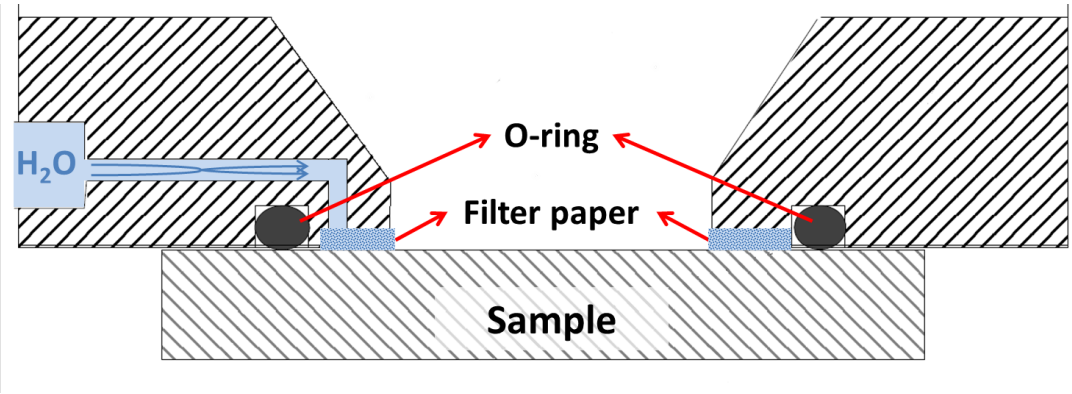

FIGURE 3.1: Schematic figure of Avesta Cell bottom with distilled water inlet to avoid crevice corrosion.

As discussed in 1.2.1 and shown in figure 1.1 the three-electrode cell consists of a working electrode, a counter electrode and a reference electrode for measuring the potentials and current densities on the sample. With use of a Luggin capillary the local potential close to the surface can be measured. For this setup a platinated titanium counter electrode with a silver/silver chloride reference electrode is used [33]. This silver/silver chloride electrode reference potential of -0.047 V versus *Saturated Calomel Electrode* (SCE) [34]. The Avesta cell with its electrodes is shown schematically in figure 3.2.

3.2 Sample Preparation

Samples were grinded up to grid 1200 silicon carbide paper before or after the heat treatment, depending on the goal of the measurement. When grinded the samples were cleaned with acetone and placed for 5 minutes in a sonic bath to remove surface particles and dried in air afterwards.

3.3 Polarization Curves

Polarization measurements were done with a step rate of 0.15 mV from -0.5 V with relation to the open-circuit potential. The standard electrolyte used was a 3.5% NaCl

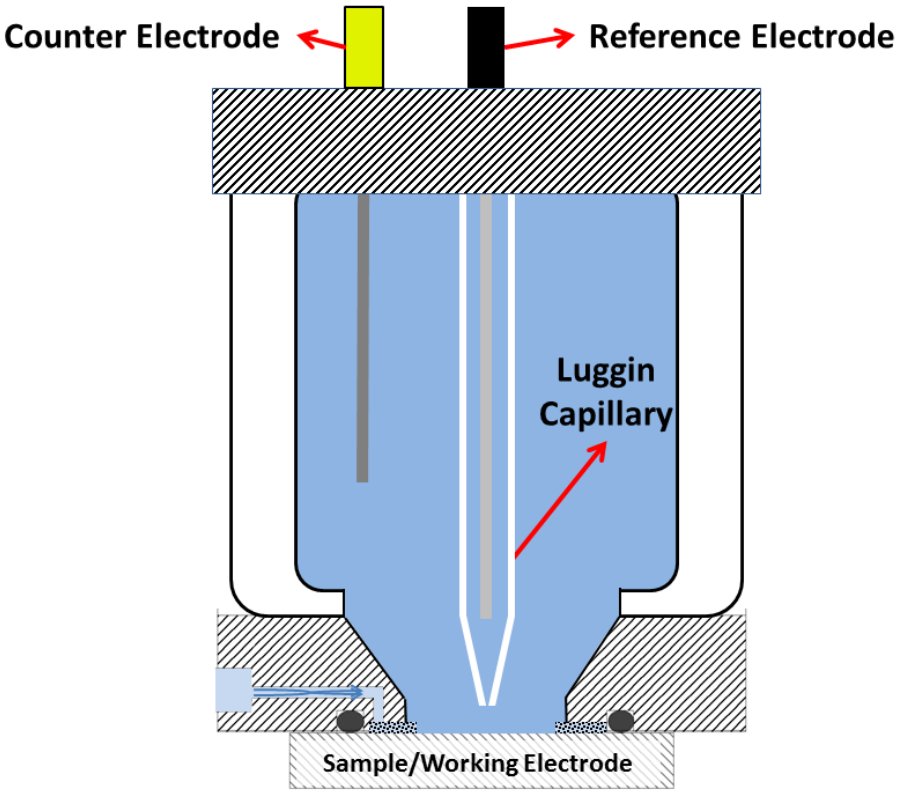

FIGURE 3.2: Schematic figure of Avesta Cell with it's electrodes; working electrode or sample, silver/silver chloride reference electrode and platinum counter electrode.

solution by mixing solid analytical sodium chloride with distilled water, for some measurements different concentrations were used. The samples were pre-treated with a potential of -0.5 V vs. Ag/AgCl to remove initial passive layers and the OCP was measured for 30 minutes subsequently [4, 6, 22].

In graph 3.3 an OCP measurement is shown of a polished AISI 420 sample (as received) that was pretreated with a -0.5 V potential for 30 minutes. From the graph it can be obtained that equilibrium state is reached after approximately 30 minutes.

3.4 Open-circuit Potential

OCP measurements are used study the electrochemical characteristics of the surface of the sample. Depending on the goal of the measurement the samples were grinded. If the characteristics of the grown oxides on the surface of the sample were studied, clearly the sample was not grinded and only cleaned in the same manner as for polarization measurements. The open-circuit potential was measured by disconnecting the counter electrode and measure the potential between the working electrode (sample) and the electrolyte compared to the reference electrode in the same electrolyte, see for further

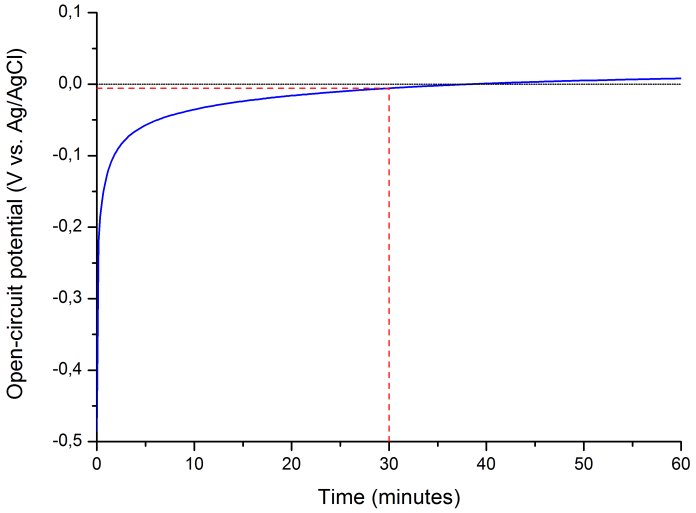

FIGURE 3.3: OCP measurement in time after a pretreatment of -0.5V vs Ag/AgCl of a polished AISI 420 sample in 3.5% NaCl solution.

explanation 1.2.1. In potentiodynamic polarization tests the OCP is measured for 30 minutes after a pre-treatment of 30 minutes at a potential of -0.5 V. After this stabilization as we see in figure 3.3 the polarization curve was measured relative to this stable OCP.

Chapter 4

Results

4.1 Carbides and Polarization Testing

In order to validate the results found with the electrochemical setup, the experiment of Lu et al. was repeated, i.e. variation of the tempering temperature. As discussed in section 2.1 increasing the tempering temperature increases the number and the size of the carbides. This leads to larger and more Cr depleted zones causing earlier breakdown of the passive film affecting the pitting potential. Samples were hardened for 45 minutes and tempered for 2 hours. Their specific heat indicated by the label, e.g. samples hardened at 1050 °C and tempered at 400 °C are indicated with 1050-400. After heat treatment the samples were grinded up to 1200 to remove any initial surface oxides. In potentiodynamic polarization measurement first the sample is pretreated with a -0.5 V potential for 30 minutes to remove the initial. The OCP is measured for 30 minutes, see 3.3 for the complete method.

Samples hardened on 1050 °C and tempered at 400 °C are indicated with 1050-400. Samples were hardened for 45 minutes and tempered for 2 hours. The obtained results are shown in figure 4.1. The As Received sample gives zero-situation, compared to this sample the pitting potential will increase or decrease when the carbides are dissolved or increased in number and size depending on the heat treatment. Starting with the lowest tempering temperature of 250 °C we see that this treatment results in the highest pitting potential. This indicates a uniform and strong passive layer that shows breakdown at high potentials. With increasing the temperature to 400 °C the pitting potential decreases and for 600 °C even further.

These results are in agreement with the model discussed in section 2.1 that assigns Cr depletion zones as the main factor for passive layer breakdown. The hardening

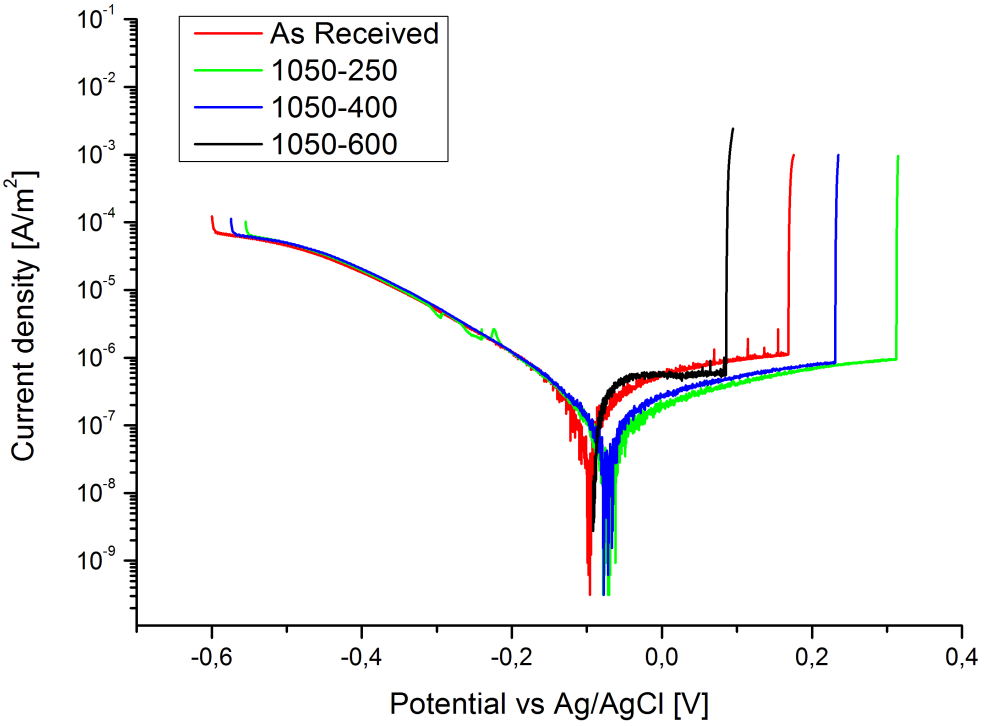

FIGURE 4.1: Potentiodynamic polarization curves of AISI 420 samples with different tempering temperatures; as received, 250 °C, 400 °C and 600 °C for 2 hours in 3.5% NaCl aqeous solution at room temperature.

treatment dissolves partly the initial present carbides into the matrix, increasing the pitting potential. Increasing tempering temperatures increase the number and sizes of the carbides and so decreases the pitting potential. In addition the current density in the passive region increases for higher tempering temperatures. Again the depletion zones are covered with thinner passive layers and cause better charge transfer for the anodic reactions, hence a higher current density.

4.2 Surface Oxides and Polarization Testing

Depending on the heat treatment and its environment, different oxides will grow on the surface of the stainless steel samples [30]. To study these oxides, samples were grinded up to 1200 prior to the heat treatment in order to preserve the new formed oxides for polarization measurements.

4.2.1 Iron Oxides

By tempering at lower temperatures in air, iron oxides are formed on top of the chromium oxide passive layer [7]. To study the influence of these iron oxide formation at the surface, AISI 420 samples were prepared by tempering in air and polarization measurements were conducted.

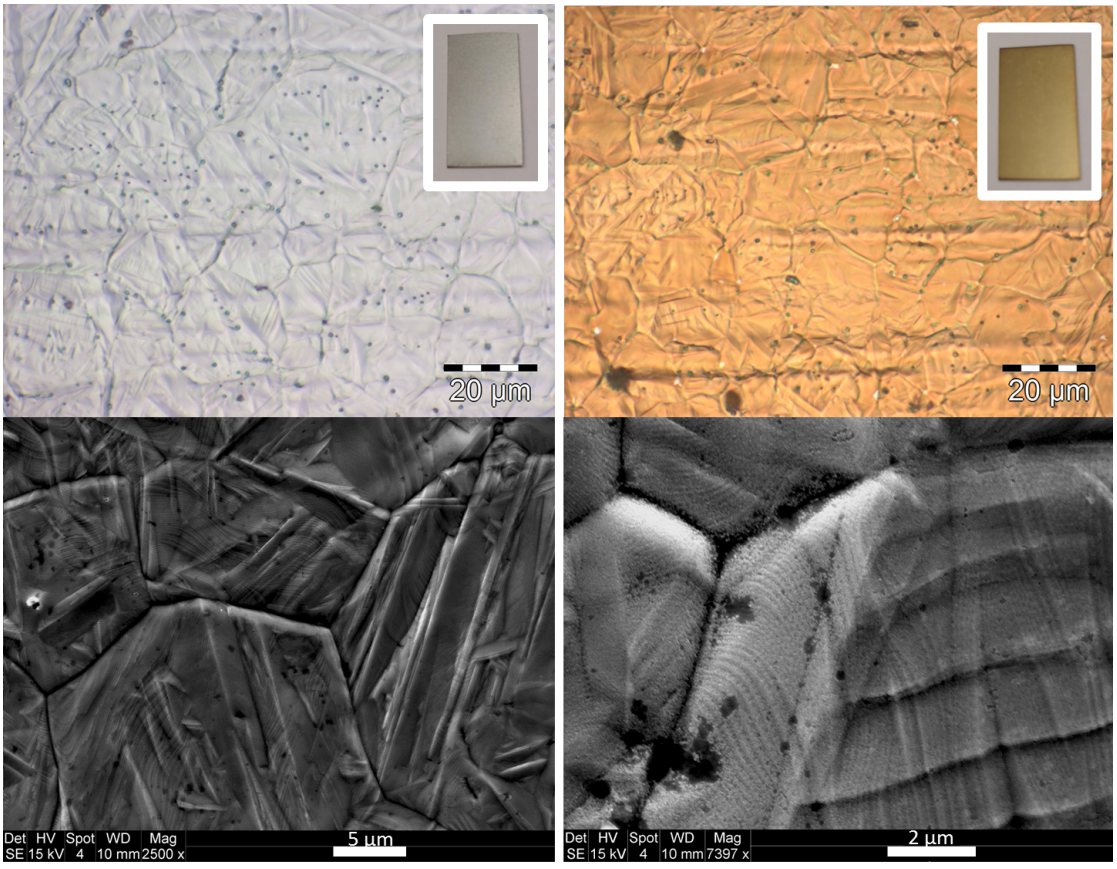

FIGURE 4.2: Left: Optical and SEM images of surface of AISI 420 sample after hardening at 1050 °C and before tempering. Right: Optical and SEM images of surface of AISI 420 sample after hardening at 1050 °C and tempering at 300 °C for 2-4 hours. The optical images are from a samples tempered 300 °C for 4 hours. The SEM images are from a samples tempered at 300-400 °C for 50 minutes.

In the optical and SEM images of figure 4.2 the surface is shown of samples before (left) and after tempering in air (right) at low temperatures (300-400 °C). Before tempering the surface has a blank appearance, after tempering at 300 °C for 4 hours the colour has clearly changed to orange/gold. On the SEM pictures we can see that this corresponds at micro-scale to a white coloured layer on top of the original surface that was visible before tempering, indicating charging particles, probably due to the badly conducting oxide layer. Junqueira et al. [35] estimated that this gold color on stainless steel correspond to a iron oxide layer thickness of around 300 nm. To check if this gold colour on these samples was also caused by an iron oxide layer a sample was studied with EDS. By

removing the oxide layers with a high negative voltage of -1 V for 30 minutes, tow domains are identified: with and without a gold coloured surface, see figure 4.3. In the results of the EDS we see that the oxygen (O) atomic percentage for the gold surface is around 15% where it is 12% for the blank surface in the middle. These results together makes it very likely that the gold surface indicates a iron oxide layer, which could be around 300 nm thick.

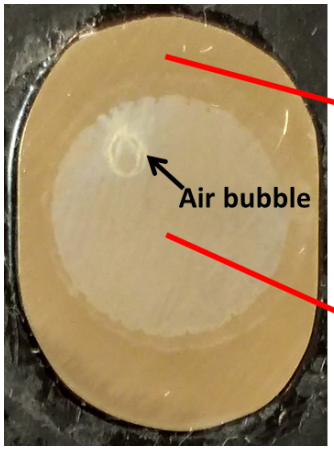

Element	Wt %	At %	Inte. Error
C K	3.23	11.98	0.59
O K	5.44	15.16	0.29
FeL	91.33	72.86	0.14
Total	100.00	100.00	

Element	Wt %	At %	Inte. Error
C K	3.59	13.50	0.56
O K	4.27	12.04	0.35
FeL	92.14	74.46	0.15
Total	100.00	100.00	

FIGURE 4.3: Sample with in the middle a circle of the removed oxide layers by applying -1V potential for 30 minutes. The blank steel next to the gold coloured surface is clearly visible. With EDS the chemical composition is compared.

The passive behaviour of the gold-ironoxide layers were studied by 2 samples, prepared in duplo. Both received the same hardening treatment of 1050 °C for 45 minutes. Both were polished to grid 1200 and were tempered in air at 250 °C, one for 20 minutes and one for 2 hours (250-20 and 250-120 respectively). After the heat treatment a polarization test was done, the duplo sample was grinded again up to grid 1200 again. The results are shown in figure 4.4. The purple and blue colored curves indicate the polished samples and therefore shows the passive behaviour of the sample without the iron oxide layer. This curve is comparable to what we have seen in figure 4.1. The pitting potentials are comparable and the current density in the passive region is a little bit lower for the sample 250-120 (tempered at 250 °C for 20 minutes).

For the unpolished samples (red and green curves) there is much more noise for the passive region with small currents. Also the current density is more than 10 times smaller. We concluded from figure 4.2 that air tempering leads to a relative thick iron oxide layer. Since oxides have a low conductivity this causes a lower current density. Connected to measuring these low currents is the relative high noise, measuring smaller currents make the noise more significant. In addition for the unpolished sample there is a big difference in pitting potential. For the unpolished 250-20 sample pitting starts even after the polished sample around 400 mV. For the unpolished 250-120 sample

this happens earlier than the polished sample, around 200 mV. Two phenomena can contribute to that; carbide growth and a thicker iron oxide layer.

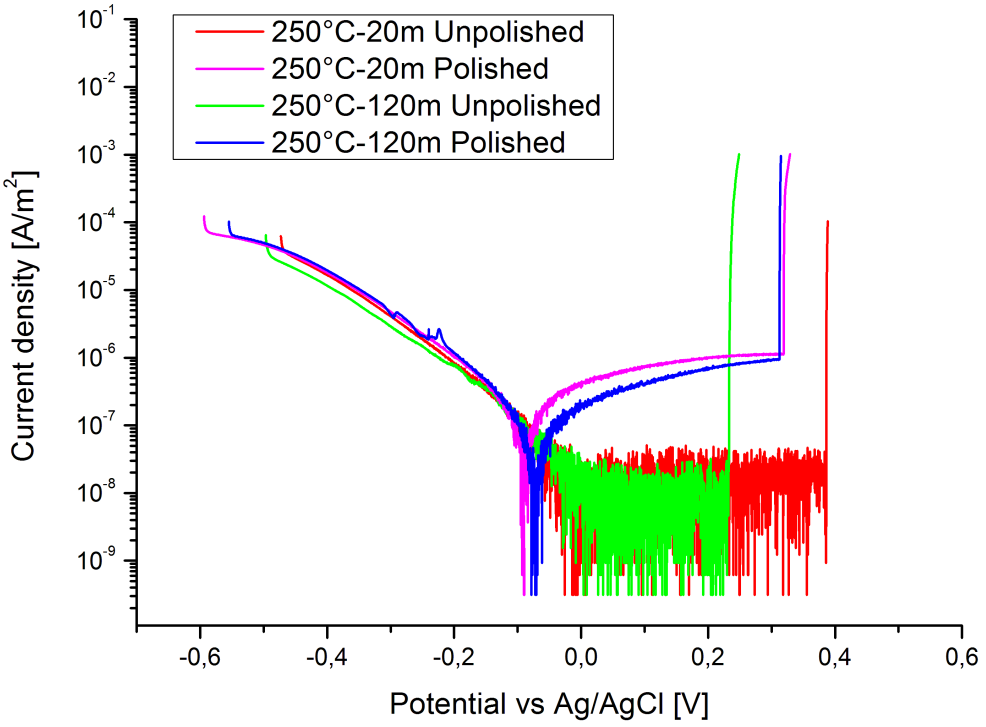

FIGURE 4.4: Potentiodynamic polarization curves of AISI 420 samples hardened at 1050 °C for 45 minutes and tempered at 250 °C for 20 minutes (250-20) and 120 minutes (250-120). Samples were compared polished and unpolished grid 1200 and measured in 3.5% NaCl aqeous solution at room temperature.

A possible explanation for the results in figure 4.4 could be given with use of the earlier shown model in figure 2.3. For the short tempered sample the iron oxide film acts as a extra or thicker passive layer, decreasing the current density and increasing the pitting potential. However when this layer becomes thicker it enhances pitting in the same way as crevice corrosion. Lu et al. suggested that the passive layer is thinner on top of the depletion zone around the chromium carbide. So when the iron oxide starts to grow the around the carbides these depletion zones are at the bottom of well in the relative thick iron oxide layer. This well separates the anodic area and the cathodic area in the same way as a crevice or pit to enhance corrosion [1]. This process is schematic given in figure 4.5

From this we conclude that iron oxides layer, grown during tempering in air, lowers the current density due to low conductivity of the oxide. For short tempering (20 minutes) the iron oxide layer enhances the passive behaviour. For longer tempering (120 minutes),

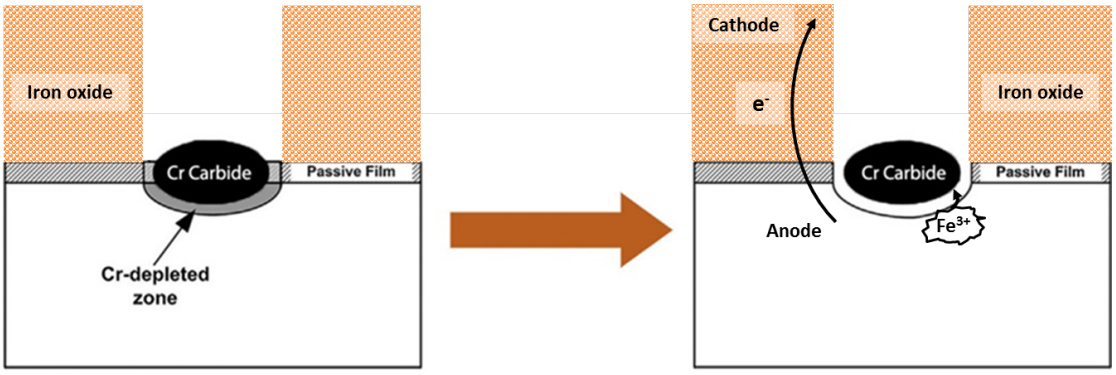

FIGURE 4.5: Schematic figure of iron oxide grown on top of the passive layer. Due to to this relative thick iron oxide, the depletion zone at the bottom of the well becomes more sensitive for pitting corrosion. The well is seperating the anode and the cathode enhancing pitting corrosion. Adapted from [3].

probably giving thicker iron oxide layers, the current density decreases again slightly but the pitting potential decreases.

4.2.2 Chromium Oxides

Since the passive layer consists of chromium oxides the next step was to study the influence of grown chromium oxides during tempering on the passive behaviour of the AISI 420 stainless steel during tempering [30]. To study this type of surface oxide a sample was after regular hardening (1050 °C, 45 minutes) tempered in low vacuum (P $\leq 10^{-2}$ Pa) at a temperature of 600 °C for 120 minutes. With XPS has been shown that this procedure resulted in an outer layer of only chromium oxide, as shown in figure 4.7.

The result of the polarization test is shown in figure 4.6. In addition the result of the 1050-600 sample with a grinded surface from figure 4.1 is shown to compare. First we see that the sample does not show any passive behaviour. Furthermore we see that the OCP lies much lower, around -400 mV vs Ag/AgCl. To explain the absense of the passive region we go back to the model described in 2. Here we saw that the passive layer depends on the chromium concentrations in the metal surface. Krishnaswamy et al. [36] found that tempering on high temperatures in vacuum causes chromium depletion just below the surface of the metal. Due to this depletion a passive layer is probably weak or even absent. The absence of the protective passive layer is immediately initiating pitting after the corrosion potential (OCP) is passed. This suggests that the chromium oxide grown during tempering does not fully cover the surface and therefore does not represent a passive layer.

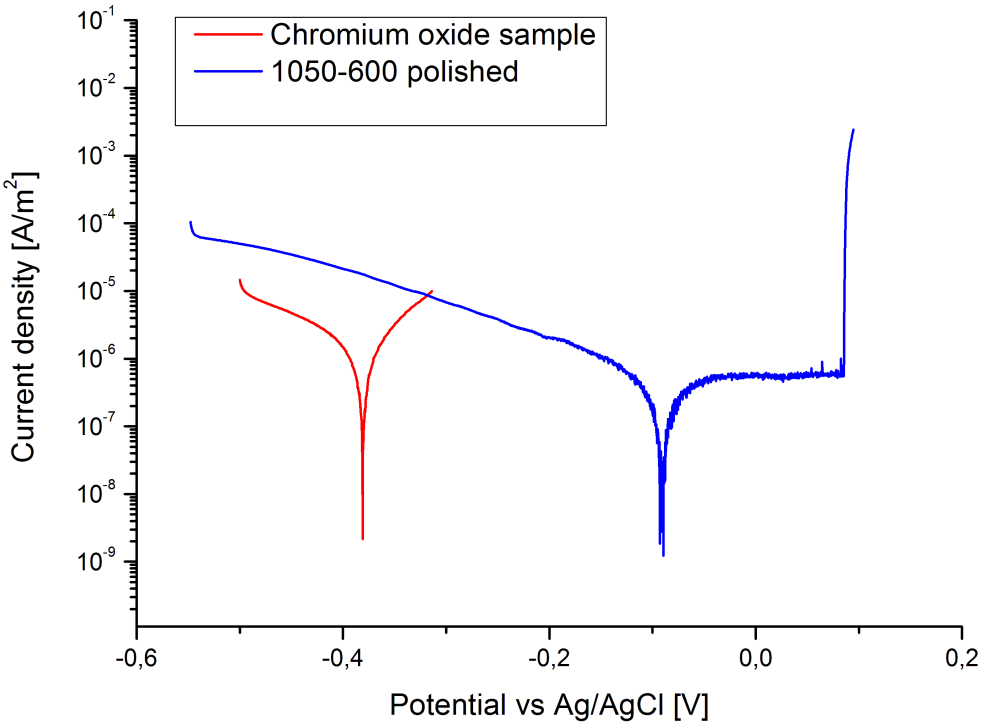

FIGURE 4.6: Potentiodynamic polarization curves of AISI 420 samples with different surfaces. Both are hardened for 45 minutes at 1050 °C and tempered at 600 °C for 120 minutes in vacuum. The polarization curve of the grinded sample is given in blue and the not grinded sample with the chromium oxide layer is given in red. Measurements were done in 3.5% NaCl aqeous solution at room temperature.

4.3 Polarization Testing of Different AISI 420 Types

Chemical composition 3 types AISI 420 stainless steel (%)

Label	C	Si	Mn	P	S	Cr	Ni	Mo	Nb
AISI420	0.32	0.15	0.30	≤0.025	≤0.010	13.7	-	-	-
AISI420 Mo	0.36	0.40	0.45	≤0.030	≤0.020	13.5	0.40	1.00	-
Nisshin	0.20-0.40	?	?	?	?	12.0-14.0	≤0.50	?	0.30-0.50

TABLE 4.1

To see if alternatives for the AISI 420 stainless steel are better corrosion resistant a polarization test was done on three different types. The compositions are shown in table 4.1. For every type a sample was prepared with a hardening heat treatment of 1050 °C for 45 minutes and grinded up to grid 1200. The results are shown in figure 4.8. From these results we see that the AISI 420 Mo type shows comparable passive behaviour as

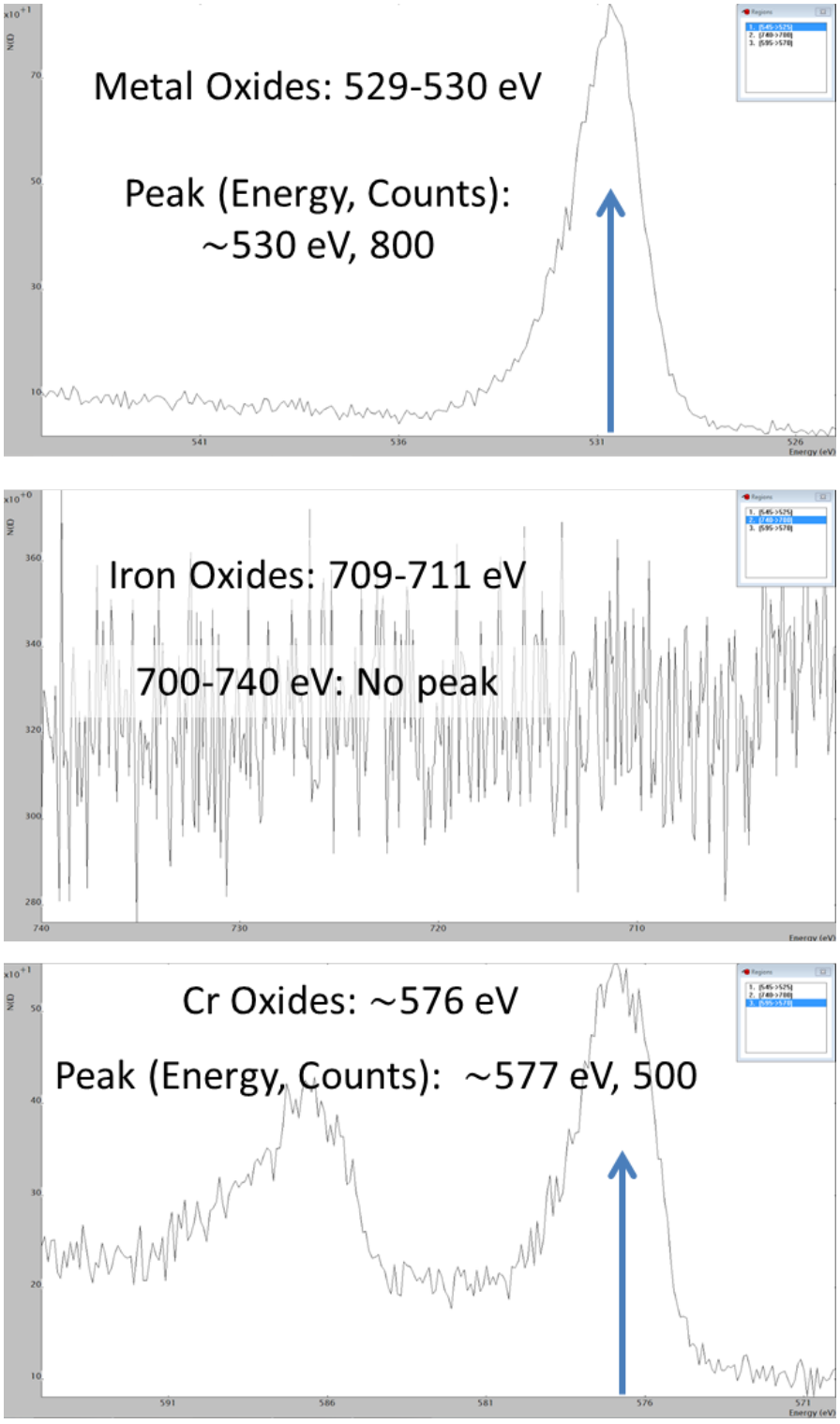

FIGURE 4.7: XPS spectrum from AISI 420 sample tempered at 600 °C in vacuum for 80 minutes. The energy ranges for oxygen, iron and chromium are shown respectively. From the peaks it was confirmed that chromium oxides were present at the surface where no iron oxides were measured.

the 'standard' AISI 420 sample used in all the previous tests. The corrosion potential or OCP lies for the AISI 420 Mo sample around 50 mV to the positive/noble direction. This indicates a thicker grown passive layer during the stabilization time previous to the polarization test, see section 1.4 and for the method used section 3.3. The pitting occurs at the same potential as the standard sample. The OCP of the Nisshin sample is close to zero at around -30 mV and therefore gives the most noble OCP of the three different AISI 420 types. The pitting potential however is lower.

AISI 420 Mo Sample

To explain the result of the AISI 420 Mo sample we have to look into the composition. Molybdenum is added to stainless steels to stabalize the passive layer [37–40]. Brigham [39] found that adding molybdenum to stainless steels is clearly improving corrosion resistance. Willenbruch et al. [38] and Olsson [37] found an enrichment of nickel and molybdenum just below the passive layer on top of the metal surface. It was found that molybdenum and nickel stabilizes the passive layer [40, 41]. From this theory the result for the AISI 420 Mo type is not surprising. The pitting potential is controlled by the number of carbides and the size of them. This is not influenced by the presence of Mo and Ni and therefore the pitting potential is almost equal to the AISI 420 standard type without Mo and Ni. The higher OCP could be caused by these stabilizing elements since the OCP depends on the present passive layer.

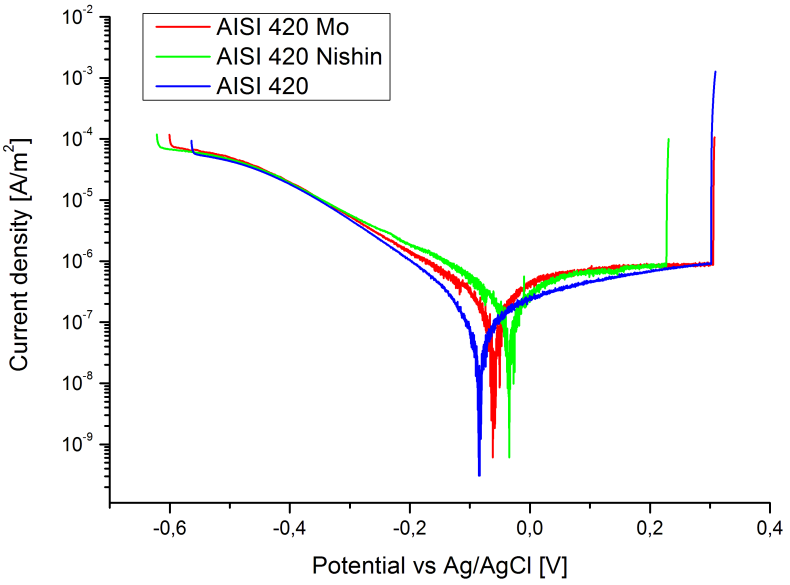

FIGURE 4.8: Potentiodynamic polarization curves of AISI 420 samples of different types hardened at 1050 °C for 45 minutes. Samples were grinded up to grid 1200 and measured in 3.5% NaCl aqeous solution at room temperature.

Nisshin Sample

From table 4.1 we see that the another element is added to the metal compared to the previous discussed AISI 420 types; niobium (Nb). Niobium is used in low concentration in martensitic stainless steels to increase strength and corrosion resistance by preventing chromium-carbide formation since Nb has strong affinity with carbon [1, 42]. However, the polarization test of the Nisshin sample clearly shows early breakdown and therefore a lower pitting potential.

Moroishi et al. [43] studied the effect of niobium on the corrosion resistance of chromium stainless steels. They found that a low concentration of Nb (<0.5%) causes a lówering of the oxidation resistance. We also see in graph 4.8 that the Nisshin sample has a increased OCP relative to the other types. Again this could be attributed to the presence of Nb. Seo et al. [44] found an enrichment of Nb in the passivated stainless steels, from this they suggest that Nb plays a role in the stability of the passive film. These studies are just examples where different mechanisms involving Nb are suggested. However, the exact mechanisms are still studied and part of discussion [45, 46]. Therefore it is hard to tell what mechanisms, involving Nb, cause the electrochemical behaviour in this case.

Conclusively these results show that alloy elements do change the electrochemical characteristics of the AISI 420 stainless steel. Molybdenum and nickel seem to influence the stabilization of the passive layer but not the moment of breakdown of the passive layer. Literature suggests that niobium is involved in the carbide formation but also in the passive layer formation. The mechanism have different effects on the electrochemical behaviour and depend on the concentration. From this it is hard to tell what mechanism causes the specific passive behaviour of our sample.

4.4 Polarization Testing of Mirror Polished Samples

In the previous results we saw that the combination of bulk material characteristics, as the carbide density and size, and the surface oxides lead to specific passive behaviour. To be able to study this closely we prepared *mirror polished* samples where the surface is polished down to 0.25 micron before tempering. The tempering was done at 250 °C for 20 minutes in air to grow a iron oxide layer again. To vary the amount of carbides a sample was hardened for 45 minutes at 1050 °C or used *as received (AR)*. We know from 4.1 that hardening at this temperature for this time lowers the concentration of carbides relative to the number of carbides in the AR sample. In this way we have a combination of different carbide concentration in the metal substrate with on top grown surface iron oxides. The results of the polarization curve are shown in figure 4.9.
The blue line represents a grinded (1200) AR sample for reference. To start we take a

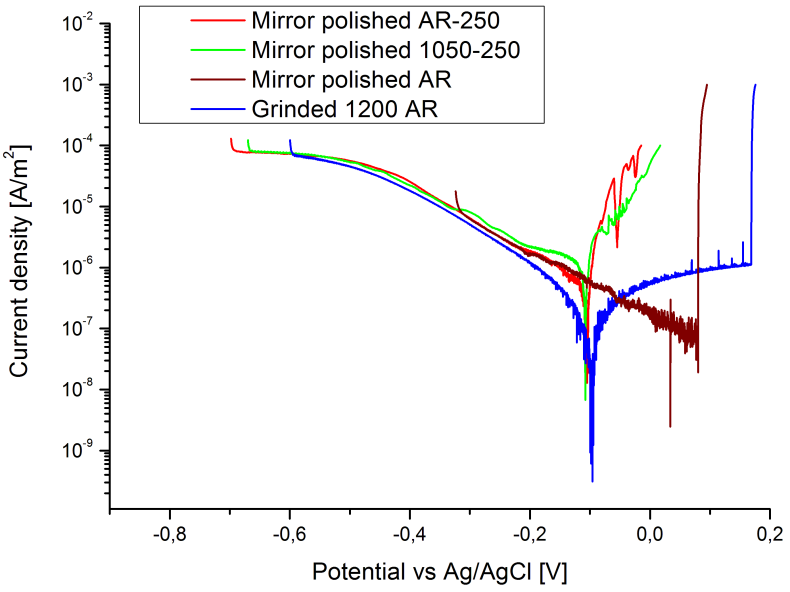

FIGURE 4.9: Potentiodynamic polarization curves of AISI 420 samples hardened at 1050 °C for 45 minutes (label: 1050) or used as received (label: AR). Mirror Polished was done before tempering at 250 °C for 20 minutes (label: 250). Measured in 3.5% NaCl aqeous solution at room temperature.

look at the red and the green curve, AR and hardened at 1050 °C respectively. Both show a OCP comparable to the reference sample, but a passive region is absent. Pitting immediately occurs. To check if this behaviour was caused by the iron oxide or the polishing a mirror polished AR sample was measured (brown curve) without tempering it. This sample shows a even more peculiar curve, especially if we take into account that the only difference between the grinded AR sample (blue) and the mirror polished AR sample (brown) is the polish method/grade. There is some kind of passive region, the current density is low and decreases if the potential increases but pitting starts to occur at a lower potential compared to the grinded AR sample. So something happened after polishing that is diminishing or even completely impair the passive behaviour. To check this an optical microscope was used with polarized light to study the surface and make carbides visible.

In figure 4.10 we see that after the polarization test was done pitts appeared that weren't there before. The red circles indicates pitts that appeared at a point on the surface without a carbide nearby. The arrows point out pitts that appeared on locations where carbides (bright spots) were visible before the polarization test. This is very likely due to the previous discussed depletion zones around carbides. The picture of the surface of the mirror polished sample that is made before the polarization test shows already excisting dark spots that look like the pitts we see after the test. This could explain

the absence of the passive behaviour in the curves in figure 4.9. If the surface is already damaged by pitts the passive layer will be interrupted and therefore more sensitive to pitting corrosion.

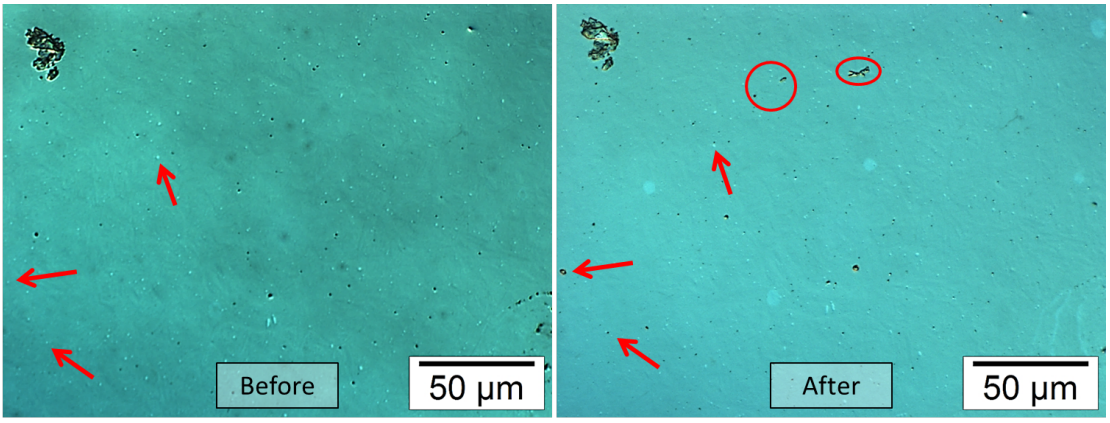

FIGURE 4.10: Mirror polished (1/4 micron) surface of AISI 420 sample before and after a polarization test was done.

In conclusion, the mirror polished samples clearly show different passive behaviour. In the case of the presence of an iron oxide layer on the surface the samples show no passive behaviour at all. For the AR sample the passive behaviour is abnormal and pitting occurs for lower potentials then a grinded with grid 1200 sample. This means that mirror polishing affects the passive behaviour. Optical examination of the surface suggests that the surface is already affected by some kind of pitts before the polarization test. This could diminish the passivation.

Chapter 5

Discussion and Conclusion

5.1 Discussion

The measurement done and discussed in 4.1 confirmed that the our setup gives comparable results as we have seen in literature [4]. Increasing the tempering temperature increases the number of carbides and causes a lowering in pitting potential. Therefore we were able to model the corrosion behaviour of this AISI 420 martensitic stainless steel. For this experiment the same parameters and methods were used as Lu et al. [4] did. In this way the experiment provided us reference data for the more novel type of measurements done later on.

Based on the results and the literature a model was suggested as presented in section 2.1 for the metal bulk material. The chromium depletion zone around the chromium carbides cause weak spots for the passive layer, decreasing the pitting potential. However, the studies done by Lu used additional techniques, like XRD and TEM, to get a complete picture of the way the carbides and the depletion zones are related to the heat treatment [6, 22, 25]. For instance, their study showed that there is some point where formation of micro-carbides cause an íncrease in pitting potential. This was not observed for the four different heat treatments used in this research but therefore can't be excluded from the possibilities. This could play a role for the experiments we did with the surface oxides or the different AISI 420 types. For the experiments with the surface oxides we used different tempering temperatures, environments, duration and alloying elements. These parameters do influence what kind of carbides are grown and in what way they are formed [42, 47]. Following this argument the given model, where chromium carbide formation is related to the passive behaviour, does not cover situations where different types of carbides are formed due to other alloying elements like niobium or specific heat treatments where micro-carbides are formed.

Based on the model for the bulk metal where the passivation highly depends on the carbides we studied the influence of grown surface oxides during tempering. The results showed that the iron oxide lowered the current density. This could be explained due to a reduced conductivity of oxides in the same way the passive layer works [3]. The effect on the pitting potential was not found in literature. A possible explanation is given in 4.2.1, where it is suggested that the relative thick iron oxide layer compared to the passive layer creates a kind of well around the carbides and enhancing pitting. For longer tempering this iron oxide grows further, leading to deeper wells. Another possibility is that the iron oxide is fuller grown, surrounding more carbides and leading to móre wells. This could be studied with use of optical observation and sputtering techniques to measure the packing of the iron oxide depending on tempering time. For this experiment also the number of measurements should be increased. There is a possibility that the pitting potential shows large variation due to the presence of the iron oxide. Based on these two measurements it is hard to tell if there is a systematic change of the pitting potential or that the pitting potential is scattered just like the current density shows some kind of noise. What is for sure is the lowering of the current density due to the grown iron oxide, this could be beneficial for corrosion resistance but therefore the effect on the pitting potential should be studied more extensively. If we better understand the consequences of tempering in air, leading to oxidized surfaces we can tune the heat treatment to desired material characteristics.

From the experiment, where the chromium oxide layer was grown by tempering at higher temperatures (600 °C) in vacuum, we learned that tempering can also completely diminish the passive behaviour of this material. Of course normally this is not a desired feature, but from this we can learn something about the way a chromium oxide is connected to passive behaviour. The passive layer that protects the stainless steel consists of mainly chromium oxides [28]. However it seems that this chromium oxide can also heavenly harm the passivation. By studying the way these chromium oxide grow and sometimes promote and sometimes diminish the passivation we can learn about the passivation mechanism involving Cr.

That brings us to the measurements done with the AISI 420 samples with the added alloy elements Mb, Ni and Nb. For the AISI 420 Mo sample, molybdenum and nickel were added to the alloy of this stainless steel. These elements are used to stabalize the passive layer [37, 40]. However, based on the theory we discussed where carbides are the main factor for defining the moment of passive layer breakdown, we did not expect big differences in polarization curves. This is because the formation of carbides are not influenced by these elements. However niobium does influence the carbide formation but at the same time effects the passive layer, as discussed in literature [43–45]. Still the exact mechanisms are not clear involving niobium, therefore it is unclear what mechanism is

dominant in this result leading to a higher OCP but a lowered pitting potential. When a stainless steel containing Nb is used, one should take into account that testing the sample on corrosion characteristics is not sufficient to know there behaviour in a certain environment. For now it is hard to model the material and it's dependency on the concentration of Nb.

The mirror polished samples showed unpredicted (non)passive behaviour. By comparing a mirror polished sample (0.25 micron) with a rougher grinded sample (grid 1200) we measured completely different electrochemical behaviour. Combined with the optical images we found already present defects/pitts on the surface. These could work as already present holes in the passive layer and therefore an absent passive region in the potentiodynamic test. If this is the case the mirror polishing method should be tuned to overcome this problem and be able to study the connection between surface oxides and the bulk material. This was the goal of these sample preparation, by taking away the roughness we would be able to couple the surface oxides and the carbides to the passive behaviour in more detail. Clearly adjustment is needed but still a promising method since carbides, grain(boundaries) and pitts are clearly visible with the optical microscope. In this way they can be connected to the polarization curves measured.

5.2 Conclusions

This brings us to the conclusions of this report. This report gives more insight in the relation of carbides, heat treatment and alloy elements to the electrochemical behaviour of the AISI 420 martensitic stainless steel. Especially the influence of these parameters on the passive behaviour is discussed and possible explanations are given. The main conclusions will be given per experiment.

Carbides and Polarization Testing
The hardening stage dissolves carbides into the matrix. During the tempering stage these carbides are able to grow again and increase in number and size for higher tempering temperature or time. These carbides are chromium enriched leading to depletion zones around in the matrix around the carbide. The depletion zones are covered with a thinner passive layer leading to early breakdown of the passive behaviour. Therefore, increasing the tempering temperature or time, decreases the pitting potential.

Surface Oxides and Polarization Testing
The presence of air during tempering at lower temperatures (250 °C) causes a growth of iron oxides layer on top of the sample surface. These oxides are bad conductors and lead lower current densities in combination with a change in the pitting potential.

Depending on the tempering time this pitting potential is higher or lower than a sample with a grinded surface, removing the gold coloured iron oxide layer. Suggested is that this has to do with the relative thick iron oxide layer compared to the passive layer. This creates a kind of well around the carbide enhancing the pitting when the dept of the well increases.

When chromium oxides are grown by tempering at higher temperatures (600 °C) an absence of the passive behaviour in the polarization curve is measured. The growth of a thick chromium oxide layer, that is blue colored, causes a depletion of chromium at the metal surface. Due this depletion the passive layer can hardly be formed or is at least weaker. Therefore pitting starts immediately to occur after the corrosion potential is reached.

Polarization Testing of Different AISI 420 Types

Alloy elements influence not only the mechanical characteristics but also the corrosion resistance. This was measured with use op polarization tests on different types of AISI 420 stainless steel with different added alloying elements. Nickel and molybdenum are stabilizers leading to a more stable passive layer but these do not have an effect on the pitting potential. Since, as said, this depends on the carbides. However an small increase in the OCP was observed after the stabilization time, possibly caused by these stabilizing elements.

Niobium however is involved in more complex mechanisms, influencing the carbide growth and the passive layer. Therefore the change of the pitting potential and OCP is hard to assign to the niobium. Clearly more experiments are needed to model the passive behaviour of this alloying element. However for all the elements it is important to realize that elements affecting the passive layer do not overcome the cause of pitting (depletion zones) and vice versa. A balance is needed and could be depicted with using polarization curves as part of the tuning process.

Polarization Testing of Mirror Polished Samples

Mirror polishing affected the passive behaviour or even diminishes it. No clear explanation for that is found. Some damages or pitss were observed after the polishing and before the testing. These could halt the passivation at that point and therefore no passive region will be measured. To be sure what these damages at the surface are and there cause, more techniques should be used to be sure of the cause of this deviating behaviour.

5.3 Future Research

Based on the results of this research project suggestions for further research will be given and discussed.

Detailed research on the carbide formation during hardening and tempering
To get a better understanding of the relation between the carbide formation and the corrosion resistance, especially the pitting potential, a better insight is needed to model the influence of hardening and tempering. In this research we did not take a close look to the types of carbides that were formed, their sizes and density. To better predict the corrosion resistance a precise relation between carbide type, size and density is needed.

Alloying elements were found influencing the carbide formation. If these elements are used to improve or stabalize the passive layer for example, the effect of these elements on carbides should also be understood. Especially the role of niobium in carbide formation and passivation desires further research.

Effect of thickness of iron oxides, grown during tempering in air, on the electrochemical behaviour
In the results we have seen that the tempering time influences the moment of pitting. For shorter times it seems to increase the pitting potential, for longer tempering time a decrease in pitting potential was observed. To understand the dependency of the electrochemical behaviour on these iron oxides, more experiments are needed where time and temperature are varied. In this way the thickness of the layer can be related to the pitting potential.

A closer look the chromium oxides
For the chromium oxide layer that was grown at higher temperatures in vacuum we saw that the passive behaviour diminished or the pitting potential decreased. To get a clear picture what is causing this behaviour the formation of this chromium oxides needs to be studied more closely. Is the depletion of chromium in the metallic surface indeed the cause, how is the layer packed and why is it not able to act as the chromium oxides in the passive layer? Is this passive layer still present or not?

Study the dependency on the polishing method When the samples were mirror polished the passive behaviour evanesced. To find and solve the reason for this the damaged on the surface that were found after polishing should be investigated. Since these features are small in size ($\lesssim 1$ μm) and the charging surface, normal electron microscopy was not sufficient. Varying the last polish steps and check with optical microscopy can give an indication if indeed the polishing is the cause. Considering the size of the abnormal features, the cause could be corrosion or maybe carbides that detached from

the surface. Still, this is speculating since no analyzing techniques that were used gave a clear indication.

In general, to fully understand the materials corrosion characteristics and it's dependency on the different heating stages, the research combines different techniques. These techniques give information about, nano-, micro- and macro-scale properties. To get a clear insight, the influence of processing parameters on nano-scale mechanisms should be related to the more general, macro-scale characteristics.

Bibliography

[1] Dumenico Surpi, Vittorio Bonsechi, Marco Boniardi, and Andrea Casaroli. *Stainless Steels*. Gruppo Lucefin. Italy, 2011.

[2] International Stainless Steel Forum (ISSF). Stainless steel in figures 2016, Jan 2016.

[3] Pierre R Roberge. *Corrosion engineering: principles and practice*. McGraw-Hill New York, 2008.

[4] S-Y Lu, K-F Yao, Y-B Chen, M-H Wang, X Liu, and X Ge. The effect of tempering temperature on the microstructure and electrochemical properties of a 13wt.% cr-type martensitic stainless steel. *Electrochimica Acta*, 165:45–55, 2015.

[5] A Nasery Isfahany, H Saghafian, and G Borhani. The effect of heat treatment on mechanical properties and corrosion behavior of {AISI420} martensitic stainless steel. *Journal of alloys and compounds*, 509(9):3931–3936, 2011.

[6] S-Y Lu, K-F Yao, Y-B Chen, M-H Wang, Na Chen, and Xue-Yuan Ge. Effect of quenching and partitioning on the microstructure evolution and electrochemical properties of a martensitic stainless steel. *Corrosion Science*, 103:95–104, 2016.

[7] GGKLA Betz, GK Wehner, L Toth, and A Joshi. Composition-vs-depth profiles obtained with auger electron spectroscopy of air-oxidized stainless-steel surfaces. *Journal of Applied Physics*, 45(12):5312–5316, 1974.

[8] Marcel Pourbaix. *Atlas of electrochemical equilibria in aqueous solutions*. National association of corrosion engineers, 1974.

[9] Cynthia G Zoski. *Handbook of electrochemistry*. Elsevier, 2006.

[10] Louis L Scribner. *The measurement and correction of electrolyte resistance in electrochemical tests*, volume 1056. ASTM International, 1990.

[11] Walther Nernst. Zur kinetik der in lösung befindlichen körper. *Z. phys. Chem*, 2: 613, 1888.

[12] Milton Stern and Al L Geary. Electrochemical polarization i. a theoretical analysis of the shape of polarization curves. *Journal of the electrochemical society*, 104(1):56–63, 1957.

[13] VS Muralidharan. An insight into the origin of corrosion potential-a critical review. *Bulletin of electrochemistry*, 18(4):179–186, 2002.

[14] Anil V Virkar, Jong Chen, Cameron W Tanner, and Jai-Woh Kim. The role of electrode microstructure on activation and concentration polarizations in solid oxide fuel cells. *Solid State Ionics*, 131(1):189–198, 2000.

[15] David Linden. *Handbook of batteries and fuel cells*. McGraw-Hill Book Co., 1984.

[16] Northeast Waste Management Officials' Association (NEWMOA). Imerc fact sheet mercury use in batteries, Jan 2010. URL http://www.newmoa.org/prevention/mercury/imerc/factsheets/batteries.cfm.

[17] Susan J Kerber and John Tverberg. Stainless steel: surface analysis. *Advanced materials & processes*, 158(5):33–36, 2000.

[18] S Jin and A Atrens. Passive films on stainless steels in aqueous media. *Applied Physics A*, 50(3):287–300, 1990.

[19] N Alonso-Falleiros and S Wolynec. Correlation between corrosion potential and pitting potential for aisi 304l austenitic stainless steel in 3.5% nacl aqueous solution. *Materials Research*, 5(1):77–84, 2002.

[20] Alberto Velázquez-del Rosario, Armín Mariño-Pérez, and Maritza Mariño-Cala. Análisis de la soldabilidad del acero inoxidable martensítico a 240 s41500 mediante ensayos de simulación de ciclos térmicos. *Minería & Geología*, 31(2):80–94, 2015.

[21] Ilyas Uygur, Husnu Gerengi, Yusuf Arslan, and Mine Kurtay. The effects of cryogenic treatment on the corrosion of aisi d3 steel. *Materials Research*, 18(3): 569–574, 2015.

[22] Si-Yuan Lu, Ke-Fu Yao, Yun-Bo Chen, Miao-Hui Wang, Yang Shao, and Xue-Yuan Ge. Effects of austenitizing temperature on the microstructure and electrochemical behavior of a martensitic stainless steel. *Journal of Applied Electrochemistry*, 45(4):375–383, 2015.

[23] William Fortune Smith. *Principles of materials science and engineering*. McGraw Hill Book Co., New York, NY, 1986.

[24] Robert E Reed-Hill and Reza Abbaschian. *Physical metallurgy principles*. Brooks/Cole Engineering Division Monterey, Calif, USA, 1973.

[25] Si-Yuan Lu, Ke-Fu Yao, Yun-Bo Chen, Miao-Hui Wang, and Xue-Yuan Ge. Influence of heat treatment on the microstructure and corrosion resistance of 13 wt pct cr-type martensitic stainless steel. *Metallurgical and Materials Transactions A*, 46(12):6090–6102, 2015.

[26] Svante Arrhenius. Über die reaktionsgeschwindigkeit bei der inversion von rohrzucker durch säuren. *Zeitschrift für physikalische Chemie*, 4:226–248, 1889.

[27] PF King and HH Uhlig. Passivity in the iron-chromium binary alloys. *The Journal of Physical Chemistry*, 63(12):2026–2032, 1959.

[28] R Kirchheim, B Heine, H Fischmeister, S Hofmann, H Knote, and U Stolz. The passivity of iron-chromium alloys. *Corrosion Science*, 29(7):899–917, 1989.

[29] K Asami, K Hashimoto, and S Shimodaira. An xps study of the passivity of a series of iron—chromium alloys in sulphuric acid. *Corrosion Science*, 18(2): 151–160, 1978.

[30] RO Adams. A review of the stainless steel surface. *Journal of Vacuum Science & Technology A*, 1(1):12–18, 1983.

[31] R Ovarfort. New electrochemical cell for pitting corrosion testing. *Corrosion Science*, 28(2):135139–137140, 1988.

[32] R Ovarfort. Critical pitting temperature measurements of stainless steels with an improved electrochemical method. *Corrosion Science*, 29(8):987–993, 1989.

[33] Bank Elektronik. Bank elektronik datasheet avesta electrochemical cell, 2016.

[34] Louis Meites. Handbook of analytical chemistry. *Soil Science*, 96(5):358, 1963.

[35] Rosa Maria Rabelo Junqueira, Célia Regina de Oliveira Loureiro, Margareth Spangler Andrade, and Vicente Tadeu Lopes Buono. Characterization of interference thin films grown on stainless steel surface by alternate pulse current in a sulphochromic solution. *Materials Research*, 11(4):421–426, 2008.

[36] SV Krishnaswamy, SB McLane, and EW Müller. Effect of annealing on the surface composition of stainless steel 410. *Journal of Vacuum Science & Technology*, 11(5):899–902, 1974.

[37] Claes-Olof A Olsson. The influence of nitrogen and molybdenum on passive films formed on the austenoferritic stainless steel 2205 studied by aes and xps. *Corrosion Science*, 37(3):467–479, 1995.

[38] RD Willenbruch, CR Clayton, M Oversluizen, D Kim, and Y Lu. An xps and electrochemical study of the influence of molybdenum and nitrogen on the passivity of austenitic stainless steel. *Corrosion science*, 31:179–190, 1990.

[39] RJ Brigham. Pitting of molybdenum bearing austenitic stainless steel. *Corrosion*, 28(5):177–179, 1972.

[40] J.L Polo, E Cano, and J.M Bastidas. An impedance study on the influence of molybdenum in stainless steel pitting corrosion. *Journal of Electroanalytical Chemistry*, 537(1–2):183 – 187, 2002.

[41] J.M. Bastidas, C.L. Torres, E. Cano, and J.L. Polo. Influence of molybdenum on passivation of polarised stainless steels in a chloride environment. *Corrosion Science*, 44(3):625 – 633, 2002.

[42] J. R. Davis. *Corrosion of Weldments.* ASM International, 2006.

[43] Taishi Moroishi, Hisao Fujikawa, and Hirobumi Makiura. The effect of carbon, zirconium, niobium, and titanium on the oxidation resistance of chromium stainless steel. *Journal of The Electrochemical Society*, 126(12):2173–2182, 1979.

[44] Masahiro Seo, Gunnar Hultquist, Christofer Leygraf, and Norio Sato. The influence of minor alloying elements (nb, ti and cu) on the corrosion resistivity of ferritic stainless steel in sulfuric acid solution. *Corrosion Science*, 26(11): 949957–955960, 1986.

[45] Teija Sipola, Tuomas Alatarvas, Eetu-Pekka Heikkinen, and Timo Fabritius. Determination of alloying elements ti, nb, mn, ni, and cr in double-stabilized ferritic stainless steel process sample using an electrolytic extraction method and separate analysis of inclusions. *Metallurgical and Materials Transactions B*, 46(4): 1775–1781, 2015.

[46] Nguyen Dang Nam and Jung Gu Kim. Effect of niobium on the corrosion behaviour of low alloy steel in sulfuric acid solution. *Corrosion Science*, 52(10): 3377 – 3384, 2010.

[47] C. R. Das, S. K. Albert, A. K. Bhaduri, V. Thomas Paul, G. Panneerselvam, and Arup Dasgupta. Study on tempering behaviour of {AISI} 410 stainless steel. *Materials Characterization*, 100:81 – 87, 2015.